MEMS & BioMEMS

Chip-Scale Quadrupole Mass Filters for a Micro Gas Analyzer

K. Cheung, L. F. Velasquez-Garcia, A. I. Akinwande
Sponsorship: DARPA

REFERENCES

[1]   M. Geear, R.R.A. Syms, S. Wright, and A.S. Holmes, "Monolithic MEMS Quadrupole mass spectrometers by deep silicon etching," *Journal of Microelectromechanical Systems*, vol. 14, no. 5, pp. 1156-1166, Oct. 2005.

[2]   J.J Tunstall, S. Taylor, R.R.A. Syms, T.Tate, and M.M. Ahmad, "Silicon micromachined mass filter for a low-power, low-cost quadrupole mass spectrometer," in *Proc. IEEE Eleventh Annual International Workshop on Micro Electro Mechanical Systems*, 1998, pp. 438-442.

[3]   L.F. Velazquez-Garcia, K. Cheung, and A.I. Akinwande, "A versatile MEMS quadrupole platform for portable mass spectrometry using the first and second stability regions," *Journal of Microsystemchanical Systems*, vol. 17, no. 6, pp. 1430-1438, Dec. 2008.

[4]   K. Cheung, L. F. Velásquez-García, A. I. Akinwande, "Fully Batch-Fabricated Linear Quadrupole Mass Filters", *Technical Digest of the 2008 IEEE Solid-State Sensors, Actuators, and Microsystems Workshop*, Hilton Head Island SC, USA, pp. 316-319

In recent years, there has been a desire to scale down linear quadrupoles. The key advantages of this miniaturization are the portability it enables and the reduction of pump-power needed due to the relaxation on operational pressure. Various attempts at making MEMS-based linear quadrupoles have met with varying degrees of success [1]-[3]. Producing these devices involved some combination of precision machining or microfabrication followed by electrode assembly. For miniature quadrupole mass filters to be mass-produced cheaply and efficiently, the electrode assembly should be removed from the process.
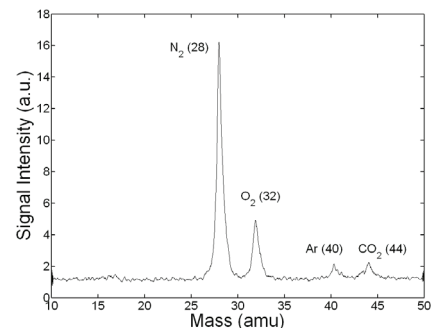
A chip-scaled quadrupole mass filter comprising a planar design and square electrodes was conceived, fabricated, and tested. Rectangular electrodes were utilized since this is the most amenable geometric shape for planar microfabrication. This deviation from the conventional round rod geometry required optimization and analysis, which was conducted with Maxwell 2D and MATLAB [4]. The fabrication process consists of thermal oxidation, the use of DRIE to define the features, and the fusion bonding of five patterned silicon wafers. This relatively simple process flow furthers the case for mass-production of these devices. A completed device measures 33 x 15 x 4 mm^3 and contains integrated ion optics as shown in Figure 1.

This non-conventional design introduces non-linear resonances that degrade the peak shape in the mass spectrum. Reported work with linear quadrupoles shows improved peak shape by operation in the second stability region [3]. Characterization of the device was conducted using FC-43, a standard calibration compound, and air as the analytes. The MuSE-QMF demonstrated a mass range of 250 amu using the first stability region and a minimum peak width of 0.7 amu in the second stability region. The main peaks for air (nitrogen, oxygen, argon, carbon dioxide) can be clearly distinguished in Figure 2.

In future work, we plan on modifying the processing and the mask layout to improve device performance. The design and fabrication concepts of this device can be expanded into arrayed configurations for parallel analysis and aligned quadrupoles operated in tandem for enhanced resolution.

FIGURE 1: Fabricated micro-square electrode quadrupole mass filter (MuSE-QMF) next to a U.S. quarter.

FIGURE 2: Mass spectrum for air using the MuSE-QMF driven in the second stability region at 2 MHz.

Tactile Sensors and Actuators for Smart Surface Applications

M. E. Swanwick, S. M-L Pfaendler, A. J. Flewitt, A. I. Akinwande
Sponsorship: Gates-Cambridge Trust, Nokia Research Center Cambridge UK

REFERENCES

[1] S.H. Dalal, "Zinc Oxide Nanowires and their Applications," Ph.D. thesis, University of Cambridge, Cambridge, UK, 2008.

[2] A. R. Rachamim; S. H. Dalal; M. E. Swanwick; A. J. Flewitt; W. I. Milne, " Quantitative Investigation of the Factors Affecting the Hydrothermal Growth of Zinc Oxide Nanowires," presented at *2009 MRS Spring Meeting*, San Franscisco, CA, April 2009.

[3] Z. L. Wang, "Novel Nanostructures of ZnO for Nanoscale Photonics, Optoelectronics, Piezoelectricity, and Sensing," *Appl. Phys. A*, vol. 88, pp 7 – 15, 2007.

[4] I. Pouprev, S. Maruyama, and J. Rekimoto, "Ambient Touch: Designing Tactile Interfaces for Handheld Devices," *Computer-Human Interactions (CHI2002)*, vol. 4, pp. 51 – 60, 2002.

[5] A. Nashel and S. Eazzaque, "Tactile Virtual Buttons for Mobile Devices," *Computer-Human Interactions (CHI2003): New Horizons, Short Talk: Haptic Interfaces*, pp. 854 – 855, April 2003.

Novel tactile sensor and actuator devices using zinc oxide nanowires have been developed to enhance the interaction between people and their environment for smart surface applications. Both the sensor and actuator device use the piezoelectric effect of zinc oxide (ZnO) nanowires. The devices are based on a cross-bar network comprising a top and bottom array of electrodes around a composite of vertically grown nanowires and an insulating polymer. This cross-bar network allows for individually addressable locations for both sensing and actuation. The results for the tactile pressure sensor show a clear spike in current when an insulating tip is placed on and removed from the surface (Figure 1). This result is compared to controls including a touch on the adjacent cross electrodes and testing another device without wires. Both tests show at least an order of magnitude difference in current between the control and the pressure sensor.
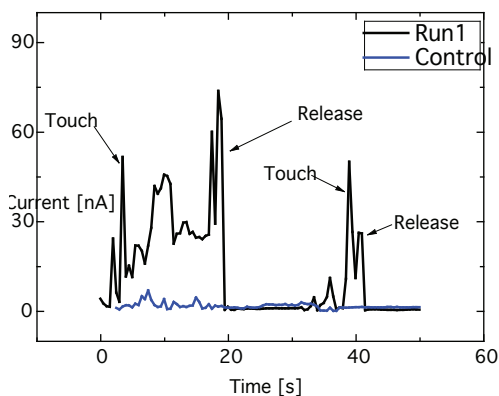
The actuator device utilizes a thin membrane of thermally grown silicon dioxide that is oscillated at resonance to induce tactile sensation. The oxide membrane is fabricated by using a deep back-side etch of a silicon wafer and utilizing the thermally grown oxide as an etch stop. The rest of the device is very similar to the pressure sensor with an electrode cross bar network and a zinc oxide nanowire polymer composite. The nanowires are grown in a furnace by chemical vapour deposition or by a low temperature hydrothermal method, producing wires of length of $1–12\mu m$ [1], [2]. The system is actuated by applying an alternating current through the top and bottom electrodes. The piezoelectric nanowires expand and contract according to the AC signal [3]. The results show a first resonance peak at 139kHz, followed by a slightly lower peak at 191kHz. The amplitude of oscillation is still not known precisely, but it is estimated to be approximately 15nm at 33V.

Currently, haptic feedback for portable electronic devices such as mobile phones is limited to vibration over a large area or the whole phone [4], [5]. This project addresses these issues by making the tactile actuators and sensors smaller than the pixel size that the finger can sense. This small pixel size leads to virtual buttons and textured surfaces that are software-controlled and infinitely variable. The long term goal of the project is to have a transparent and flexible device so that it can be incorporated into a variety of different displays and surfaces.

FIGURE 1: Tactile pressure sensor results compared with a control run. An insulated probe tip was manually pressed onto the device, as signified by the Touch and Release labels. For the control run, the tip was placed on an adjacent cross-bar and the tip was again manually placed and rubbed on the surface.
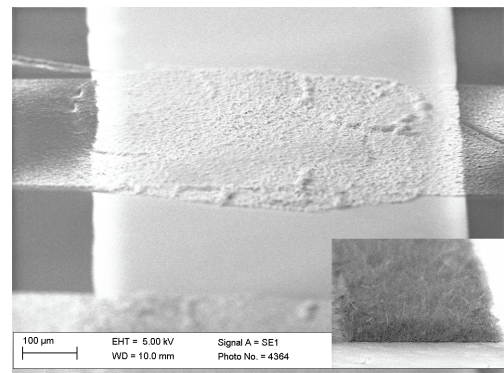
FIGURE 2: An SEM micrograph of the cross-bar activation device taken at a 70-degree angle. The device is a SiO_2 membrane with Nb electrodes and thermally grown vertical ZnO nanowires in a polymer composite. Insert in lower right: Thermally grown ZnO nanowires on Nb (the electrode is 100 μm wide for scale)
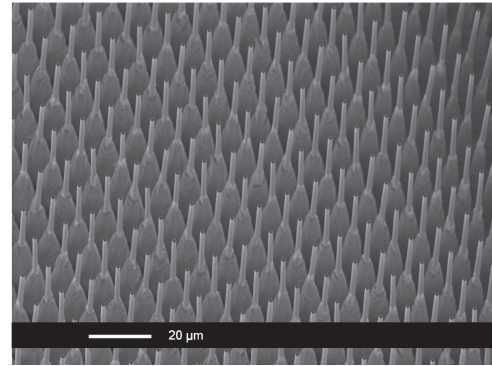
MEMS-based Plasma Probes for Spacecraft Re-entry Monitoring

L. F. Velásquez-García, A. I. Akinwande
Sponsorship: NASA

REFERENCES

[1] J. A. Stillman, F. C. Chiang, P. A. Pribyl, M. Nakamoto, W. Gekelman, and J. W. Judy, "Microfabricated Probes for Laboratory Plasmas", in *Proceedings Solid-State Sensors, Actuators, and Microsystems Workshop*, Hilton Head Island SC, pp 308 – 311, 2006.

[2] M. Wijesundara, G. Valente, W. Ashurst, R. Howe, A. Pisano, C. Carraro, and R. Maboudian, "Single-Source Chemical Vapor Deposition of 3C-SiC Films in a LPCVD Reactor I. Growth, Structure, and Chemical Characterization", *Journal of the Electrochemical Society*, Vol. 151, n. 3, pp. C210-C214, 2004.

[3] R. S. Okojie, G. M. Beheim, G. J.Saad, and E. Savrun, "Characteristics of Hermetic 6H-SiC Pressure Sensor at 600 C, in *Proceedings of the AIAA Space 2001 Conference and Exposition*, Albuquerque, NM, August 28-30, 2001 (AIAA Paper No. 2001-4652).

[4] R. S. Okojie, D. Lukco, Y. L. Chen, and D. J. Spry, "Reliability Assessment of Ti/TaSi2/Pt Ohmic Contacts on SiC After 1000 h at 600 C," *Journal of Applied Physics*, Vol. 91, no. 10, pp. 6553-9559, 2002.

[5] A. Pisano (PI), HERMIT Program at U. C. Berkeley, DARPA MTO PI Meeting, Long Beach CA, July 2007.

[6] L. F. Velásquez-García, B. Gassend, and A. I. Akinwande, "CNT-Based Gas Ionizers with Integrated MEMS Gate for Portable Mass Spectrometry Applications", to be presented at *the 15th International Conference on Solid-State Sensors, Actuators and Microsystems*, Denver, CO, USA, June 21 – 25, 2009.

NASA's strategic plan calls for a focus on advanced sensing that would assure continued safe operations. We propose a set of three cost-effective and reliable MEMS-based sensors to diagnose in real time the conditions of the plasma surrounding the spacecraft during reentry. The proposed sensors are (i) arrays of Langmuir probes, (ii) arrays of retarded potential analyzers, and (iii) arrays of GPS antennas. Each sensor is targeted to gather specific information of the plasma, and it is operated in such a way that allows fast data collection. There are reports of MEMS-based devices for plasma diagnostics such as Langmuir probes [1]. Although these sensors work, their shield is made of polyimide. Therefore, these sensors are not compatible with the high-temperature or high-density plasmas that the spacecraft encounters at re-entry. Silicon Carbide (SiC) is a semiconductor material that is very resistant to hostile environments [2]. There are current research efforts to develop SiC-based MEMS intended for harsh environments, including pressure, acceleration, temperature, and strain transducers, as well as transistors [3]-[5]. The SiC is a promising material to implement low-cost and reliable plasma diagnostics. We are exploring SiC both as a coating and as fabrication substrate. The work has focused on the Langmuir probe development. Langmuir probe densities as large as 10^6/cm^2 have been demonstrated (Figure 1). Also, fabrication experiments using a plasma-enhanced chemical vapor deposited (PECVD) SiC coatings have been conducted (Figure 2). Future research includes the development of an RPA based on an ionizer we recently developed [6] and experimental validation of the sensors.

FIGURE 1: A set of high aspect-ratio Si columns (1 μm ×1 μm × 100 μm) coated with a protective SiO$_2$ film. The tips of the columns can be used as Langmuir probes to sample the plasma every 10 μm.
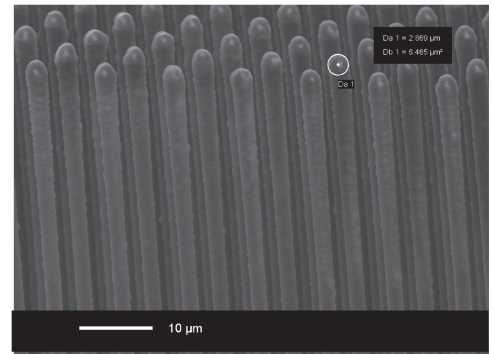
FIGURE 2: A set of high-aspect-ratio Si columns coated with a PECVD SiC film.
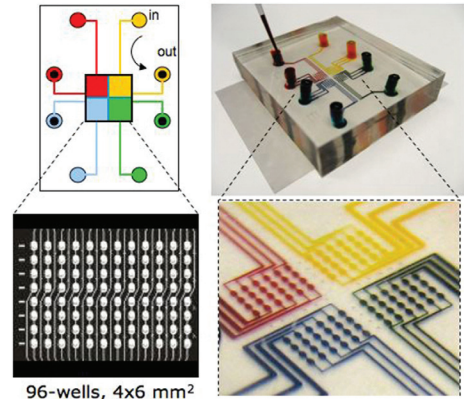
Investigating Stem Cell Dynamics Utilizing Microfluidic-based Time-lapse Imaging

G. H. Underhill, D. R. Albrecht, J. Resnikoff, S. N. Bhatia, J. V. Shah

REFERENCES

[1]   G.H. Underhill and S. N. Bhatia, "High-throughput analysis of signals regulating stem cell fate and function," *Curr Opin Chem Biol*, vol. 11, no. 4, pp. 357-366, Aug. 2007.

[2]   J. Melin and S. R. Quake, "Microfluidic large-scale integration: the evolution of design rules for biological automation," *Annu Rev Biophys Biomol Struct*, vol. 36, pp. 213-231, June 2007.

An understanding of the mechanisms underlying stem cell fate and function has recently been augmented by the application of microfabricated systems, designed to systematically probe important environmental stimuli and intrinsic genetic programs [1]. In particular, current approaches leveraging these systems aim to enhance both the spatial and temporal resolution of stem cell analysis, providing a more complete picture of dynamic stem cell processes. Microfluidics represents a promising technology for the parallel analysis of cellular responses to numerous perturbations simultaneously within a single device [2], although it can be difficult to implement in traditional biology laboratory settings. To examine the dynamics of embryonic stem (ES) cell self-renewal and differentiation, we have employed a simple microfluidics platform, without valves or specialized equipment, coupled with near-simultaneous time-lapse imaging. This integrated system incorporates a miniaturized 96-well, ~6 x 4 mm² imaging area with a variable input/output channel design and enables the interrogation of ES cell kinetics within multiple environments. We have tested the platform with both feeder-independent mouse ES cell lines as well as co-cultures of mouse ES cells with supportive mouse embryonic fibroblast (MEF) feeder layers and demonstrated self-renewal over 3-4 days of analysis. The examination of ES cells containing fluorescent protein fusions was utilized to monitor chromosome dynamics during self-renewal and to evaluate proliferation kinetics; furthermore, perturbation with an anti-mitotic agent demonstrated the dynamic response to exogenous factors within the device. Overall, these studies illustrate the capacity to dynamically assess and manipulate stem cell processes through the integration of a simple, but modular, microfluidics-based imaging platform.

96-wells, 4x6 mm²

FIGURE 1: Microfluidic device for imaging mES dynamics. The design and scheme for four independent experiments is illustrated.

FIGURE 2: The Oct4-EGFP mES cells cultured on gelatin-coated glass coverslips and imaged at 24-hr time points. The top series illustrates a field imaged at 4X magnification, containing multiple microwells. The bottom series of paired fluorescent and phase contrast images represents the indicated single well imaged at 20X magnification. Scale bars: 200 mm (top), 50 mm (bottom paired).

Direct Patterning of Metallic MEMS through Microcontact Printing

C. E. Packard, A. Murarka, V. Bulović
Sponsorship: DARPA, Hewlett-Packard

Standard photolithography-based methods for fabricating microelectromechanical systems (MEMS) present several drawbacks including expense, incompatibility with flexible substrates, and limitations to wafer-sized device arrays. We have developed a new fabrication method for rapid fabrication of large-area MEMS that breaks the paradigm of lithographic processing using a scalable, large area microcontact printing method to define three-dimensional electromechanical structures. Our PDMS Lift-Off Transfer (PLOT) involves the rapid removal of a pick-up stamp from a transfer pad to transfer a continuous metal film from the pad to the stamp. A stamp that forms the membrane suspension supports is fabricated by molding a thin layer of PDMS against a silicon master with a predefined relief. The metal membranes are deposited by thermal evaporation onto a transfer pad which has been prepared with an organic molecular release layer. To achieve transfer of the metal membrane over the supports of the device, the stamp is brought into conformal contact with the transfer pad and then released by rapidly peeling away. MEMS bridge structures, such as the ones shown in Figure 1, have been fabricated using PLOT, and their performance as variable capacitors has been characterized. In Figure 2, the capacitance of these devices increases with applied voltage, indicating mechanical deflection of the bridges due to the electrostatic force. PLOT forms MEMS structures without requiring elevated temperature processing, high pressure, or wet chemical or aggressive plasma release etches, providing compatibility with sensitive material sets for the fabrication of integrated micro- or opto-electronic/MEMS circuits. Flexible, paper-thin device arrays produced by this method may enable such applications as pressure sensing skins for aerodynamics, phased array detectors for acoustic imaging, and novel adaptive-texture display applications.
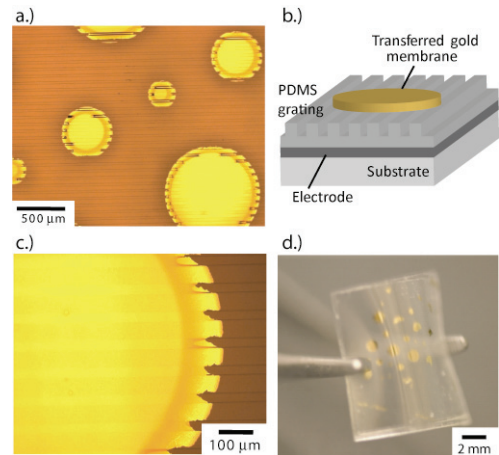
FIGURE 1: Devices formed by PLOT: optical micrographs (a. & c.), schematic (b.) and photograph of devices formed on a flexible substrate (d.)
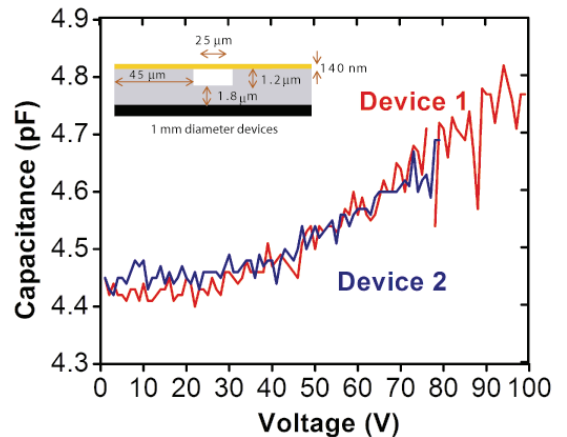
FIGURE 2: Capacitance increases with applied voltage in two devices, indicating mechanical deflection of the bridging metal film.

Design of Micro-scale Multi-axis Force Sensors for Precision Applications

M. A. Cullinan, R. M. Panas, M. L. Culpepper
Sponsorship: DoD

Multi-axis force-sensing at the micro-scale is necessary for a wide range of applications in biology, materials science, and nanomanufacturing. A three-degree-of-freedom force sensor (Figure 1) was designed that is capable of accurately and precisely measuring the adhesion forces (nanoNewtons) between biologically active surfaces. This force sensor is positioned and actuated using a Hexflex nanopositioner and Lorenz force actuators as seen in Figure 2.

In order to design high-accuracy, high-precision, multi-axis MEMS force sensors, a closed form model was developed to optimize the strain sensitivity of the MEMS force sensor. This model first sets constraints on the system due to package size, fabrication techniques, desired degrees of freedom, and force range. The layout of the flexure system is optimized to meet the kinematic and manufacturing constraints of the MEMS force sensor. The geometry of the flexures is set to maximize the strain at the sensor locations.

This model was incorporated into a thermal/electric model to fully characterize all of the inputs to the system. The resolution of the force sensor is a function of the noise from the strain sensors, the noise in the electronics, the thermomechanical noise, and the sensitivity of the strain sensors to a force input. Based on this model, the dominant noise sources are identified and the sensor system is optimized to reduce these noise sources. The thermal/electric model is also used to determine the major factors limiting the accuracy of the force sensor. In most cases, the drifts in both the electronics and sensors caused by fluctuations in room temperature were the major sources of accuracy errors. Therefore, an environmental enclosure with closed-loop control over temperature was designed and implemented. Overall, the final design of the force sensor is capable of producing sub-nanoNewton-resolution force measurements with nanoNewton-level accuracy.
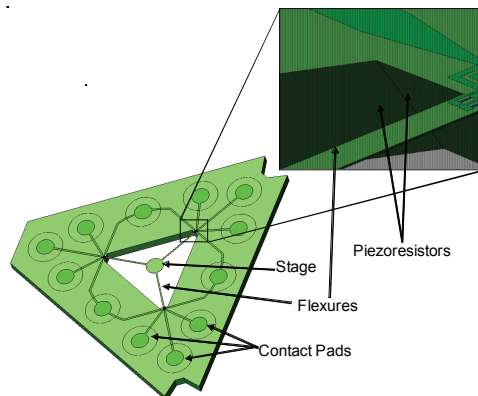
FIGURE 1: A 3-axis force sensor with polysilicon strain gauges on the flexure beams.
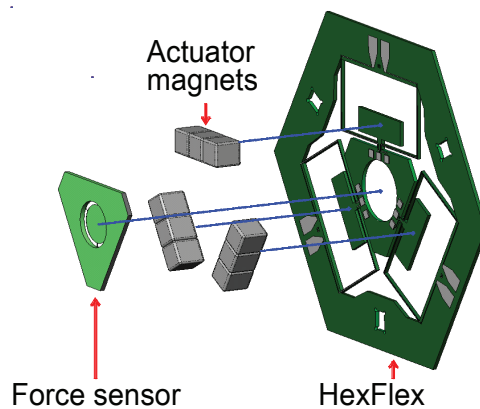
FIGURE 2: Schematic of how the force sensor actuator magnets fit on the Hexflex nanopositioner.

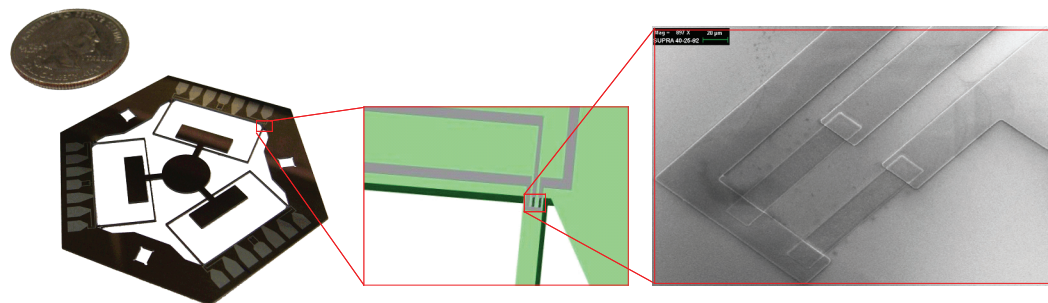# Design of a Six Degree of Freedom Nanopositioner for Use in Massively Parallel Probe-based Nanomanufacturing

C. M. DiBiasio, M. L. Culpepper
Sponsorship: NSF via OSU NSEC

REFERENCES

[1] M.L. Culpepper and G. Anderson, "Design of a Low-cost Nano-manipulator Which Utilizes a Monolithic, Spatial Compliant Mechanism," *Precision Engineering*, vol. 28, pp. 469-482, Aug. 2004.

[2] D. Golda and M.L. Culpepper, "Two-axis Electromagnetic Moving-Coil Micro-Actuator," in *Proc. of the 2006 ASME International Mechanical Congress and Exposition*, 2006.

[3] C.M. DiBiasio and M.L. Culpepper, "Design of a Meso-scale Six-axis Nanopositioner with Integrated Position Sensing," in *Proc. Fifth Annual International Symposium on Nanomanufacturing*, 2008.

In probe-based nanomanufacturing a micro-scale probe tip is used to create or measure nm-scale features. The serial nature of probe-based manufacturing dictates that practical throughput rates will require the use of two-dimensional tip arrays. These arrays must be controlled in six degrees-of-freedom to maintain parallelism with respect to the work surface. Meso-scale, 6-axis nanopositioners [1] will be needed because they (1) are lower cost ($100s US versus $10,000s), (2) possess higher bandwidth, and (3) are more thermally stable than macro-scale nanopositioners. Furthermore, their small size enables arraying many nanopositioners in a small footprint. Sensing is important as this enables closed loop position control and therefore control in a nanomanufacturing process. We have designed and microfabricated low-cost nanopositioners with nm-level accuracy and resolution that are equipped for closed-loop operation throughout a 50x50x50 μm3 work volume. Figure 1 shows the nanopositioner (less actuators [2] and electronics) that contains an integrated 6-axis piezoresistive sensing system [3]. The figure inset shows the piezoresistor arrangement, wherein a first sensor is placed along the beam's neutral axis and the second sensor is placed at the beam's edge. Both sensors are placed near the root of the cantilever where maximum device strain occurs. The neutral axis sensor experiences strain primarily from out-of-plane bending while the sensor on the edge of the beam experiences strain from in- and out-of-plane bending. Biasing these signals makes it possible to obtain in-plane and out-of-plane measurements from the sensors while keeping them located on the same face of the flexible beam. The structure of the nanopositioner was microfabricated from a 400 μm thick silicon wafer with 500 nm polysilicon piezoresistors fabricated onto the flexural beams. Each nanopositioner costs approximately $250 US and initial tests indicate the nanopositioner will have 2 nm out-of-plane resolution and 20 nm in-plane resolution.

FIGURE 1: Microfabricated six-axis nanopositioner with integrated piezoresistive sensing. The inset shows the arrangement of the piezoresistors on the flexural beams.

Magnetically-assisted Assembly, Alignment, and Orientation of Micro-scale Components

J. Diaz, D. Cheng, C. G. Fonstad, Jr. in collaboration with F. Cadieu, Queens College of CUNY, M. Zahn, MIT
Sponsorship: Vitesse Chair

The use of magnetic forces to improve fluidic self-assembly of micro-components has been investigated using Maxwell 3D to model the forces between Ni thin films on semiconductor device micro-pills and Sm-Co thin films patterned on target substrates [1]. Orienting and restraining forces on pills far in excess of gravity are predicted, and it is found that the fall-off of these forces with pill-to-substrate separation can be engineered through the proper design of the Sm-Co patterns to retain only properly oriented pills [1], [2].

Micro-scale hybrid assembly is a potentially important way of doing heterogeneous integration, i.e., of integrating new materials on silicon integrated circuits to obtain functionality not readily available from silicon device structures alone, and fluidic self-assembly is an attractive way to automate micro-scale assembly. A serious limitation of fluidic self-assembly, however, is the lack of a good method for holding properly assembled components in place and accurately positioned until all of the components have been assembled and they have been permanently bonded in place. We have shown, based on our modeling,

that suitably patterned magnetic films can be used to provide the forces necessary to retain, and to accurately orient and position, assembled micro-components.

Our motivation for pursuing micro-scale hybrid assembly is our general interest in doing optoelectronic integration, specifically of vertical cavity surface emitting lasers (VCSELS), edge-emitting lasers (EELs), and light emitting diodes (LEDs), with state-of-the-art, commercially processed Si-CMOS integrated circuits. Our ongoing research integrating these devices on silicon described elsewhere in this report provides the context for this work and illustrates the types of applications we envision for magnetically assisted self-assembly using the results of this study.

Assembly experiments to verify and demonstrate the theoretical predictions are currently in progress using two sizes of 6-μm-thick pills (50 μm by 50 μm and 50 μm by 100 μm) and a variety of magnetic thin film patterns. Recesses with different dimensions are also being studied [2].

REFERENCES

[1]   D. Cheng, "Theoretical and Experimental Study of Magnetically Assisted Fluidic Self Assembly," MEng. Thesis, Department of Electrical Engineering and Computer Science, MIT, June 2008.

[2]   D. Cheng, J. J. Rumpler, J. M. Perkins, M. Zahn, C.G. Fonstad, E. S. Cramer, R. W. Zuneska, and F. J. Cadieu, "Use of Patterned Magnetic Films to Retain and Orient Micro-Components during Fluidic Assembly," *Journal of Applied Physics*, Vol. 105, 07C123, 2009.
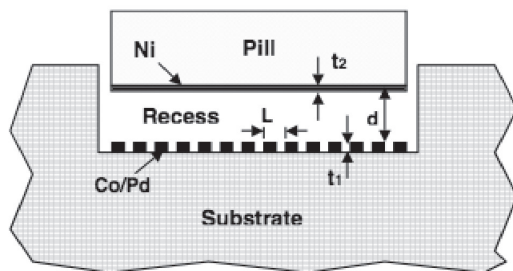
FIGURE 1: A cross-sectional cartoon illustrating the application of magnetically assisted assembly to recess integration. The variables indicated in the drawing correspond to the model used to calculate the magnetic force intensity.
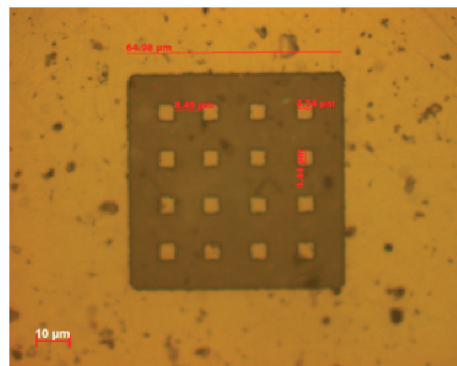
FIGURE 2: A microphotograph of a patterned samarium cobalt magnetic thin film. The abilities first to sputter-deposit and second to wet-etch thin films like this is critical to the successful implementation of magnetic self-assembly and are unique strengths of the MIT/Queens College effort.

Microfabricated Slits in Series:
A Simple Platform to Probe Differences in Cell Deformability

H. Bow, P. Abgrall, J. Han

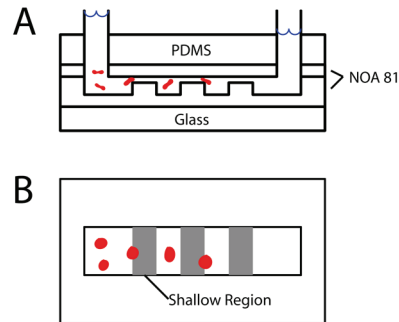Change in cell stiffness is a characteristic of blood cell diseases such as sickle cell anemia, malaria[1], and leukemia[2]. Often, increases in blood cell stiffness lead to loss of the cells' ability to squeeze through capillaries, resulting in organ failure, coma, and ultimately death. The spleen is the organ in the human body that is responsible for removing these less deformable cells. It functions by forcing cells in blood to squeeze between endothelial cells arranged like the staves of a wooden barrel.

The goal of this project is to create a microfluidic device that can quickly and accurately screen, diagnose, and treat disorders involving cell deformability. We report the creation of a microfabricated device consisting of a series of 1-2 μm-wide polymeric slits, modeled on those of the spleen, Figure 1. Using this device, we demonstrate unambiguous mobility differences between cells differing solely in stiffness.

Figure 2 shows mobility differences for red blood cells (RBCs) treated with different concentrations of GA in a 2-μm slit device. The GA acts as an amine-crosslinker, making the cell membrane and cytosol stiffer. The RBCs are slightly larger than this slit size and must deform to traverse the slit. Velocities of 0.001% GA-treated cells were within experimental error to untreated cells. The cells treated with 0.01% GA exhibited a velocity of 0 μm/s, as they were too rigid to pass through the slits. At a concentration of 0.003 %, the cells were semi-rigid and showed decreased mobility compared to the untreated cells. Cell size was observed to be the same throughout the range of GA concentrations.

These results demonstrate that increased membrane stiffness can cause statistically significant mobility differences through a series of slits. Additionally, the low-cost aspect of this device makes it ideal for on-site disease (e.g., malaria) screening in resource-poor settings.

REFERENCES

[1]   J. P. Shelby, J. White, K. Ganesan, P. K. Rathod and D. T. Chiu, "A microfluidic model for single-cell capillary obstruction by Plasmodium falciparum-infected erythrocytes," *Proc. Natl. Acad. Sci. U. S. A.,* vol. 100, pp. 14618-14622, December 9, 2003.

[2]   M. J. Rosenbluth, W. A. Lam and D. A. Fletcher, "Force Microscopy of Nonadherent Cells: A Comparison of Leukemia Cell Deformability," *Biophysical Journal*, vol. 90, pp. 2994-3003, 2006.

FIGURE 1: A. Side view. The smallest RBC dimension is greater than the height of the slits. Therefore, RBCs must deform to get through. B. Top view.
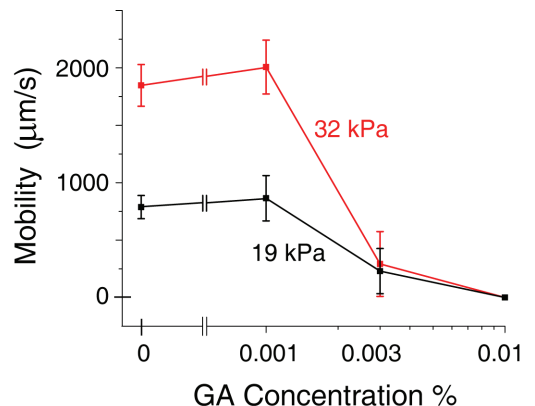
FIGURE 2: Mobility vs. GA concentration. Higher GA concentration increases cell stiffness, resulting in decreased mobility.

Microfabricated Devices for Portable Power Generation

C. H. Marton, K. Deshpande, M. A. Schmidt, K. F. Jensen

The development of portable power-generation systems remains an important goal, with applications ranging from the automobile industry to the portable electronics industry. The focus of this work is to develop microreaction technology that converts the chemical energy stored in fuels–such as light hydrocarbons and their alcohols—directly into electricity or into a different energy vector such as hydrogen. Developing devices with high energy-conversion efficiency requires addressing difficulties in high temperature operation: specifically, thermal management, material integration, and improved packaging techniques.

A catalytic combustion-based device intended for the direct conversion of thermal energy to electricity has been developed. The combustor has been designed to achieve attractive energy and power densities while addressing system challenges such as mechanically robust fluidic connections and minimal parasitic power losses related to pressurization of air. The channels of the combustor are etched using wet potassium hydroxide, which is the most economical etch technique available. Straight channels (1mm by 1mm in cross-section) are arranged in parallel and separated by 100-μm–thick silicon walls, in order to achieve low pressure drop (< 300 Pa at 10 SLPM gas flow) with significant surface area ($\sim$1 cm^2 per channel) for catalyst deposition. Two identical reactors are stacked using metal thermocompression bonding to increase reactor volume without a significant increase in exposed surface area. External gas distribution manifolds are compression-sealed to the reactor, eliminating the need for glass brazing of tubes, increasing the mechanical robustness of the device, and avoiding large pressure losses associated with flow constrictions. Platinum-on-alumina catalyst has been washcoated on the channel surfaces for the catalytic combustion of butane with air.

A combined reforming/separation device has been developed and demonstrated. The hydrogen generation unit combines a 200-nm-thick palladium-silver film with a methanol reforming catalyst (supported palladium). The catalytic combustion unit employs a supported platinum catalyst. Both units are formed in a silicon wafer by bulk silicon micromachining techniques. The energy generated in the combustion unit is efficiently transferred to the hydrogen production unit by the thermal conduction of silicon support. The system has been demonstrated to purify hydrogen at elevated pressures (up to 2 atm). Joint combustion/purification of the system has also been demonstrated, in which combustion and reforming occur simultaneously with the purification of the resulting hydrogen.
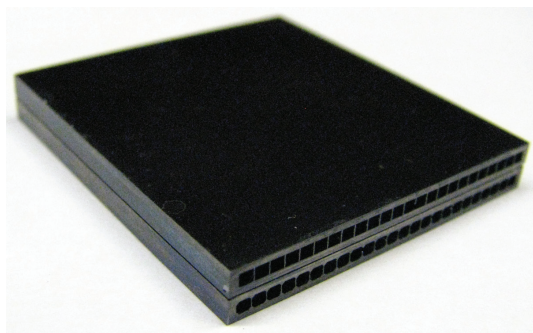
FIGURE 1: Catalytic combustion device prior to connection to the gas distribution manifold. Each of the 48 channels is 1 mm by 1 mm by 31 mm, and is separated by a 100-µm–thick wall.
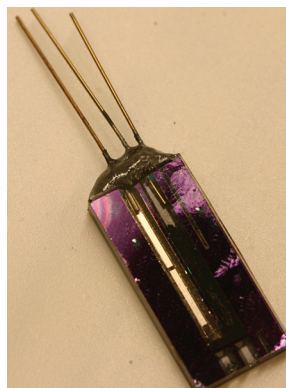
FIGURE 2: Combined reformer/separator device. The three fluidic connections are for reactant gases, combusted gases, and purified hydrogen.
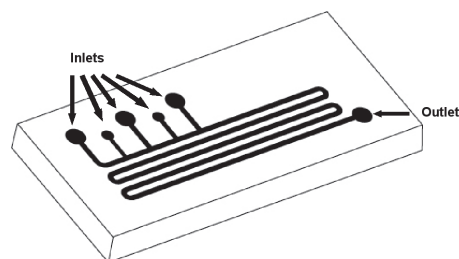
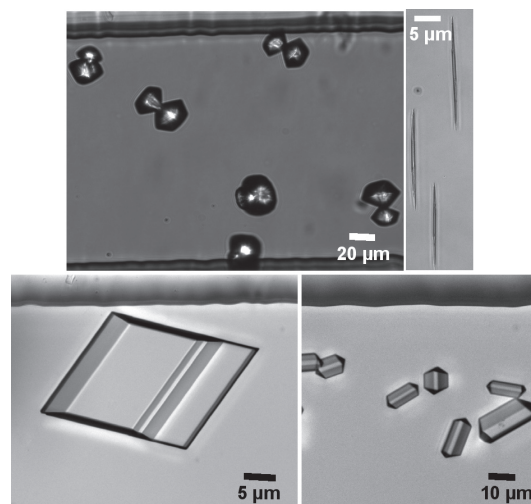# Microfluidic Systems for Continuous Crystallization

M. Sultana, K. F. Jensen

Microfluidic systems offer a unique toolset for discovering new crystal polymorphs and for studying the growth kinetics of crystal systems because of well-defined laminar flow profiles and online optical access for measurements. Traditionally, crystallization has been achieved in batch processes that suffer from non-uniform process conditions across the reactors and chaotic, poorly controlled mixing of the reactants, resulting in polydisperse crystal size distributions (CSD) and impure polymorphs. Consequently, batch crystallization suffers from reproducibility issues, increases difficulty in obtaining accurate kinetics data, and manufactures products with inhomogeneous properties. The small length scale in microfluidic devices allows for better control over the process parameters, such as the temperature and the contact mode of the reactants, creating uniform process conditions across the reactor channel. Thus, these devices have the potential to generate more accurate kinetics data and produce crystals with a controlled morphology and a more uniform size distribution. In addition, microfluidic systems decrease waste, provide safety advantages, and require only minute amounts of reactants, which is most important when dealing with expensive materials such as pharmaceutical drugs.

Figure 1 shows a microfluidic device used for crystallization; Figure 2 shows optical images of different polymorphs of glycine crystals grown inside reactor channels. A key issue for achieving continuous crystallization in microsystems is to eliminate heterogeneous crystallization–irregular and uncontrolled formation and growth of crystals at the channel surface– and aggregation of crystals, which ultimately clogs the reactor channel. We have developed a microcrystallizer using soft lithography techniques that introduce the reagents to the reactor channel in a controlled manner, preventing heterogeneous crystallization and aggregation. We have used optical microscopy *in situ* to obtain high-resolution images of crystals grown in continuous microreactors and use image analysis to derive growth kinetics of crystals of different morphologies and shapes. In addition, we have integrated an online spectroscopy tool for *in situ* polymorph detection. In summary, we have developed a microfluidic system for continuous crystallization of small organic molecules and integrated it with *in situ* detection tools for size and morphology characterization.

FIGURE 1: The microfluidic device used for crystallization.

FIGURE 2: Different sizes and shapes of glycine crystals produced in the reactor channel.
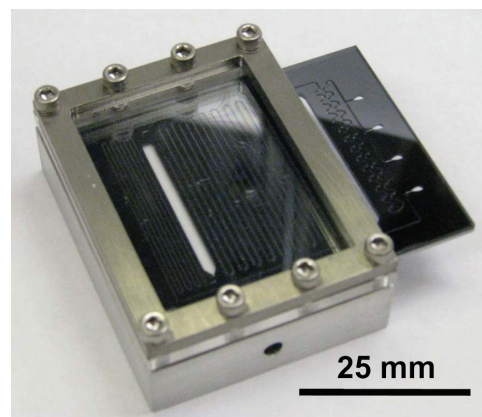
Multistep Microfluidic Systems for Synthetic Chemistry

R. L. Hartman, N. Zaborenko, H. R. Sahoo, B. C. Yen, K. F. Jensen

REFERENCES

[1]   H. R. Sahoo, J. G. Kralj, and K. F. Jensen, "Multistep continuous-flow microchemical synthesis involving multiple reactions and separations," *Angew. Chem.-Int. Edit.*, vol. 46, pp. 5704-5708, 2007.

[2]   J.G. Kralj, H.R. Sahoo, and K.F. Jensen, "Integrated continuous microfluidic liquid-liquid extraction," *Lab on a Chip*, vol. 7, pp. 256-263, 2007.

[3]   R.L. Hartman, H.R. Sahoo, B.C. Yen, and K.F. Jensen, "Distillation in microchemical systems using capillary forces and segmented flow," *Lab on a Chip*, 2009, DOI: 10.1039/b901790a.

Microchemical systems have recently gained prominence for use in reaction screening and augmentation. However, most chemical syntheses combine several reaction and work-up steps, and independently studying each step limits understanding of how they are coupled in a process. To that end, microfluidic systems have been integrated to realize multistep reaction and liquid-liquid extraction steps [1], [2]. However, other separation techniques are needed in traditional batch synthetic transformations such as filtration, evaporation, and distillation. Consequently, developing a fundamental understanding of microfluidic distillation has been undertaken.

Distillation is a ubiquitous method of separating liquid mixtures based on differences in volatility. This unit operation is fundamental to a number of industrial processes, and performing such separations in microfluidic systems is difficult because interfacial forces dominate over gravitational forces. The concept of distillation has been engineered on a silicon-based microfluidic chip as shown by the device shown in Figure 1 [3]. Microfluidic distillation is realized by establishing vapor-liquid equilibrium during segmented flow. Enriched vapor in equilibrium with liquid is then separated using capillary forces, thus enabling a single-stage distillation operation. As shown in Figure 2, separation of binary liquid mixtures (e.g., methanol (MeOH) and toluene) is made possible by carrying out microfluidic distillation. These experimental results were consistent with phase equilibrium predictions.

FIGURE 1: Fabricated distillation device with an on-chip condenser and integrated vapor-liquid membrane separator. The photograph shows a device packaged in an aluminum compression chuck for precise temperature control. [3]
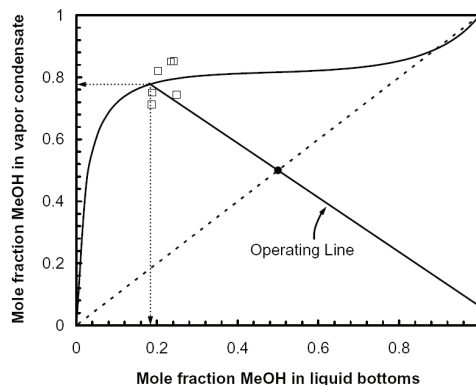
FIGURE 2: McCabe-Thiele diagram for distillation of 50:50 mol% MeOH-toluene at 70.0°C using the device shown in Figure 1. The curved line represents the phase-equilibrium of MeOH-toluene while the black squares denote multiple repeats of the single-stage enrichment. The solid straight line (i.e., operating line) represents equation (16) whereas the dashed line is y = x. [3]

Direct Printing of PZT Thin Films for MEMS

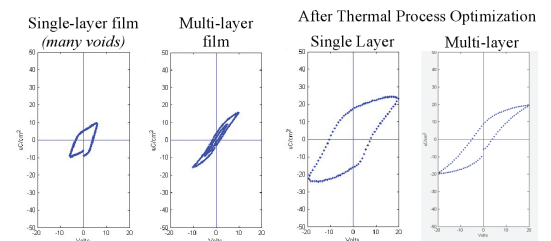S. Bathurst, H .W. Lee, S. G. Kim

In 2008-2009, we continued our work on thermal ink-jet printing of PZT [1], further optimizing the deposition process and thermal post-processing. Early work showed that modified sol-gel inks often have reduced performance due to porosity, pin holes, and void formation. Multi-layer deposition was investigated as a means to seal voids. Multiple ferroelectric capacitors were fabricated, all with approximately 400nm of printed PZT. Multi-layer films showed consistently improved dielectric properties over single-layer films, with less leakage current and higher resistivity. The continued refinement of the thermal processing profile developed in 2007-2008 lead to a 3hr pyrolysis at 400C followed by a 650C anneal in an O_2 environment. These small adjustments improved organic removal, increased film densification, and provided improved piezoelectric response (Figure 2). The remanent polarization of each capacitor was measured as metric for piezoelectric performance. Finally, printing of devices with different thicknesses on a single wafer was demonstrated, something that cannot be accomplished with conventional coating techniques. Future work includes further development of a thermal treatment for multi-layer films. The samples in figure 2 were annealed between each layer, potentially affecting the alignment of the ferroelectric domains between layers. Work on devices in which the entire stack is annealed together is ongoing. Once this annealing is accomplished, thermal ink-jet printing of PZT of the highest dielectric and piezoelectric quality will have been realized.

REFERENCES

[1]   S. Bathurst, H. W. Lee and S. G. Kim, "Direct Printing of Lead Zirconate Titanate Thin Films," in *21st IEEE International Conference on Micro Electro Mechanical Systems"*, 2008, pp 391-394.
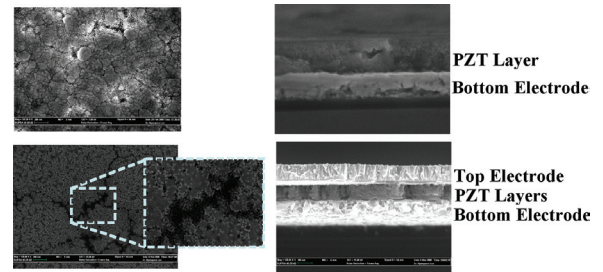
FIGURE 1: SEM images of two thermal ink-jetted PZT devices. Top: single 400nm layer; bottom: 4x100nm layers.

FIGURE 2: Performance data for four printed PZT devices showing the improvement as thermal processing improved and multi-layer deposition was begun.

Nonlinear Pie-shaped MEMS-scale Energy-harvester

A. Hajati, S. G. Kim

REFERENCES

[1]   Y.R. Jeon, Sood, J.H. Jeong, S.G. Kim, "MEMS power generator with transverse mode thin film PZT," *Sensors and Actuators A: Physical*, vol. 122, pp. 16-22, 2005.

[2]   W.J. Choi, Y. Xia, J.A. Brewer, and S.G. Kim, "Energy harvesting MEMS device based on thin-film piezoelectric cantilevers," in *Proc. of INSS05*, San Diego, CA, June 27-28, 2005.

[3]   A. Hajati and S.G. Kim, "Rectifierless Piezoelectric Micro Power Generator," *SPIE Smart Structures and Materials & Nondestructive Evaluation and Health Monitoring 2008*, San Diego, CA, 2008.

A novel nonlinear pie-shaped thin-film lead zirconate titanate Pb(Zr,Ti)O (PZT) MEMS energy-harvester has been developed. It harvests energy from parasitic ambient vibration via piezoelectric effect and converts it to electrical energy. The new nonlinear pie-shaped design tries to exploit the maximum theoretical power density of PZT for small levels of vibration and wide range of frequencies in a robust way. Contrary to the traditional designs based on cantilever high-Q oscillators which use bending strain, the new design heuristically utilizes the stretching strain in doubly-anchored beams in order to maximize the strain and power. It also provides a wide-bandwidth of operational frequency due to the system's nonlinearity and enables a robust power generation amid the unexpected change in the vibration spectrum. The device is microfabricated by a combination of surface and bulk micromachining processes in order to use the whole thickness of wafer to form a heavy proof mass. For the structural layers of the beams, 2-μm-thick, high-quality, low-stress silicon nitride is used; it is deposited using low-pressure chemical vapor deposition (LPCVD). Layers of thin-film PZT and ZrO_2 as the diffusion barrier are deposited by sol-gel spin-coating, wet-etched, and annealed to form the active area of the device. E-beam deposition and lift-off is used to place interdigitated (IDT) electrodes that extract the generated charge, exploiting the d piezoelectric mode of PZT. Deep reactive-ion-etching (DRIE) from top and back of the wafer patterns the nitride beams and silicon proof mass and finally a XeF_2 etching of silicon fully releases the device. Released devices are super-glued on Pin Grid Array (PGA) packages in such a way that the proof mass is located on top of the cavity to give it enough space for motion in response to the base vibration. The pads on the device are wire-bonded to the package's pads. Devices are heated to 100C and poled at 180kV/cm for 30 minutes using the setup shown in Figure 1. The piezoelectric properties of each device are electrically verified by Polarity/Voltage measurement (Figure 2). Currently, the poled devices are under electromechanical testing to verify their energy-harvesting characteristics.

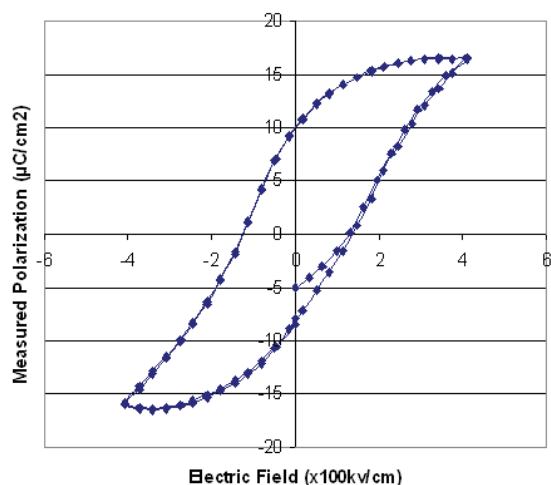**FIGURE 1:** Device is being poled.

**FIGURE 2:** The P-V curve shows a healthy piezoelectric material.

Templated Inkjet Printing for MEMS
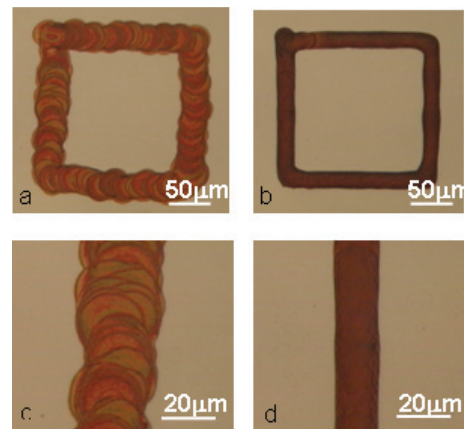
H. J. Lee, S. Bathurst, H. Lee, S. G. Kim
Sponsorship: DARPA, Hewlett-Packard, Korea Institute of Science and Technology

REFERENCES

[1]   S. Bathurst, H.W. Lee, S.-G. Kim, "Direct printing of lead zirconate titanate thin films for microelectromechanical systems," in *Micro Electro Mechanical Systems, MEMS 2008. IEEE 21st International Conference*, January 13-17, 2008, pp. 391-394.

[2]   Y. Wang, J. Bokor, A. Lee, "Maskless lithography using drop-on-demand inkjet printing method," *Lithographic Technologies VIII*. Edited by Mackay, R. Scott. *Proceedings of the SPIE*, volume 5374, pp. 628-636 (2004).

[3]   E. Lam, "Fabrication and material characterization of silver cantilevers via direct surface micromachining," Master's thesis, Massachusetts Institute of Technology, Cambridge, 2008.

Drop-on-demand (DoD) printing has shown great promise as a low-volume production method for MEMS. A new method for depositing lead zirconate titanate (PZT) piezoelectric thin films via thermal inkjet (TIJ) printing was recently reported by authors [1]. We demonstrated that well optimized printing conditions could provide thickness uniformity with less than 100-nm variation. However, the printed pattern showed more than +/- 10-μm edge (line) roughness, which is far bigger than the necessary minimum feature size for most MEMS devices. In general, the minimum possible line width created by most droplet-based deposition processes has been bigger than ~25 mm due to the possible spot resolution, and 3-5 mm roughness was demonstrated only in a research environment [2]. A pre-fabricated dam or trench can be a solution for defining fine edges by printing, which requires additional dam patterning with lithography or laser trimming and additional post-processing steps for dam structure removal [1], [3].

We show that an imprinted self-assembled mono-layer (SAM) template behaves as a wetting/non-wetting barrier for water-based inkjetted droplets and confines water-based inks within the hydrophilic region. The SAM imprinting is done by micro-contact printing with fluorinated thiol ink. The smallest droplet size tested in this work was 3pL, which could define 20-μm line roughness at best. The inkjet droplets were printed between the imprinted square patterns as shown in Figure 1. The pitch between each droplet and the dropping interval were controlled as shown in Figure 2. The left figures show the patterns without imprint guided inkjet printing and the right figures show the printing with template assistance. The pattern with imprint assisted printing shows a line roughness of less than +/- 1μm, which could not be achieved with the current inkjet printing methods.
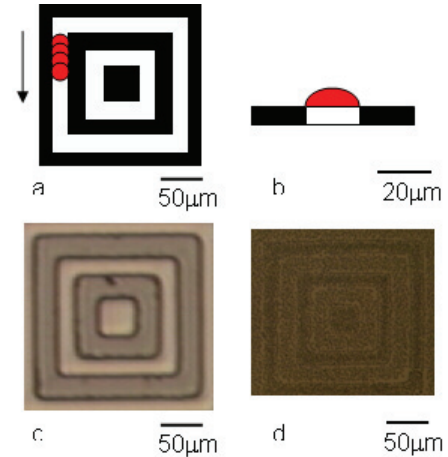
FIGURE 1: Top view (a) and cross-section view (b) of imprint guided printing; the red dot is dropped ink, white region is hydrophilic, and black is hydrophobic. A PDMS stamp (c) and invisible thiol pattern on platinum surface (d) shown by exhaled moisture

FIGURE 2: Inkjet-printed lines on untemplated surface (a) and templated surface (b). The untemplated case shows line roughness of +/- 10mm (c) and the templated case is +/- 1mm (printing condition: 3pL ink drop/ 2.5-mm pitch/ 2.0 second dropping interval).

A 1-mW, 25-Hz Vibration-energy-harvesting System
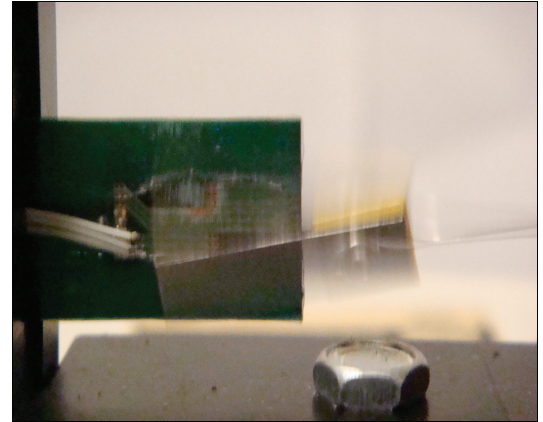
S. C. Chang, D. M. Otten, J. H. Lang
Sponsorship: DARPA

REFERENCES

[1] R. Amirtharajah and A. P. Chandrakasan, "Self-powered signal processing using vibrationbased power generation," *IEEE Journal of Solid-State Circuits, 1997 Symposium on VLSI Circuits,* 13-15 June 1997, vol. 33, pp. 687-95, 1998.

[2] S. Meninger, J. O. Mur-Miranda, R. Amirtharajah, A. Chandrakasan, and J. H. Lang, "Vibration- to-electric energy conversion," *IEEE Transactions on Very Large Scale Integration (VLSI) Systems,* vol. 9, pp. 64-76, 2001.

This project is part of the Hybrid Insect MEMS (HI-MEMS) program sponsored by the Defense Advanced Research Projects Agency (DARPA). The main objective of this program is to establish the interface between adult neural systems and external electronics. Here, insects are the first test bed, and they will be directed to fly to specific locations in real time via wireless remote control through the external electronics. In order to provide sustainable energy for the controlling on-moth electronics, a local energy-harvesting system is required. The energy-harvesting system has two major parts: the vibration-energy-harvester [1] and the DC-DC boost converter [2]. In the past 12 months, a 1-mW vibration-energy-harvester was designed, fabricated, and tested. Figure 1 shows the harvester. A DC-DC 10-mV to 1-V boost converter has also been designed and is ready for tape out. Figure 2 shows the topology of the boost converter.

The vibration-energy-harvester consists of a resonator with moving magnets and a coil. As the resonator vibrates, neodymium iron boron magnets sweep past coils through which power will be harvested. The coils are made with flexible printed-circuit technology to maximize the flux linkage and minimize the coil mass. The harvester was tested on a shaker table, which simulates the vibration of a moth. After testing, 1-mW of time average power was extracted at a mass cost of 1.067g. Work is now underway to significantly reduce the mass of the harvester.

The boost converter takes in the AC output voltage of the harvester, rectifies it to a DC voltage and boosts the voltage to 1V. The converter is a two-stage boost converter with off-chip inductors to increase the quality factor and overall efficiency. Due to the low input voltage of the harvester, synchronous rectification using low-power discontinuous comparators is employed. Spice simulation indicates that the converter can achieve 80% efficiency. The power processing switches have been laid out and are currently in the queue to be fabricated in 0.18-um CMOS process.
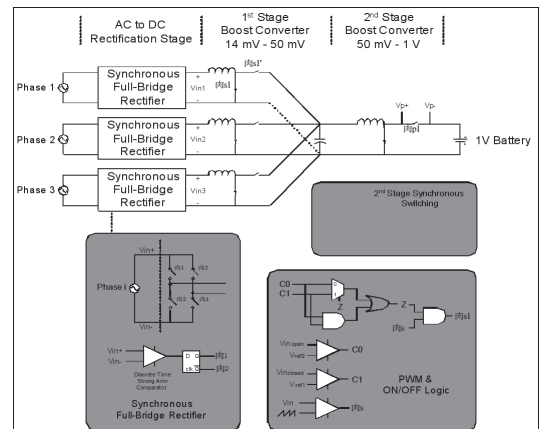

FIGURE 1: Energy-harvester system scavenging power from a shaker table that simulates the vibration of a flying moth. The harvester is capable of generating 1-mW of power from a 25-Hz, 1-mm vibration source.

FIGURE 2: Boost Converter Circuit topology consisting of three sets of first-stage boost converters with synchronous rectification. Inductors will be off-chip.

Development and Application of Distributed MEMS Pressure Sensor Array for AUV Object Avoidance

V. I. Fernandez, S. M. Hou, F. S. Hover, J. H. Lang, M. S. Triantafyllou

REFERENCES

[1]   S.P. Windsor, D. Tan, J.C. Montgomery. "Swimming kinematics and hydrodynamic imaging in the blind Mexican cave fish (Astayanax fasciatus)," *Journal of Experimental Biology*, vol. 211, pp. 2950-2959, 2008.

[2]   C. von Campenhausen, I. Riess, and R. Weissert, "Detection of stationary objects by the blind cave fish *Anoptichthys jordani* (Characidae)," *Journal of Computational Physiology A*, vol. 143, pp. 369-374, 1981.

[3]   J.C. Montgomery, S. Coombs, and C.F. Baker, "The mechanosensory lateral line system of the hypogean form of *Astyanax fasciatus*," *Environmental Biology of Fishes*, vol. 62, pp. 87-96, 2001.

A novel sensing technology for unmanned undersea vehicles (UUVs) is under development. The project is inspired by the lateral line sensory organ in fish, which enables some species to form three dimensional maps of their surroundings. The lateral line is a sensory system which measures the flow velocity and pressure distribution over the fish's surface, enabling behaviors such as collision avoidance [1] and object recognition [2]. These behaviors are related to a particular subset of the lateral line organ, which measures only the pressure gradient [3]. We report progress in fabricating a sensor array capable of measuring similar quantities as the lateral line organ.

The system consists of arrays of hundreds of pressure sensors spaced about 2 mm apart on etched silicon and Pyrex wafers. The sensors are arranged over a surface in various configurations. The target pressure resolution for a sensor is 1 Pa, which corresponds to the noiseless disturbance created by the presence of a 0.1-m-radius cylinder in a flow of 0.5 m/s at a distance of 1.5 m. A key feature of a sensor is the flexible diaphragm, which is a thin ($20\,\mu$m) layer of silicon attached at the edges to a silicon cavity. The strain on the diaphragm due to pressure differences across the diaphragm is measured. At this stage, the individual MEMS pressure sensors are being constructed and tested.

The output voltage was measured and the relative change in resistance $\Delta R/R$ for the resistors as functions of pressure were calculated (Figure 2). For a diaphragm with a width of 2.82 mm, we obtained the experimental values of $(\Delta R/R)/P$ are -2.94×10^{-7} Pa, -2.78×10^{-7} Pa, 2.52×10^{-7} Pa and 2.65×10^{-7} Pa. The theoretical value is $\pm 1.07 \times 10^{-7}$ Pa. There are several explanations for the discrepancy between theory and experiment. Regardless, the sensitivity of the sensor is better than the original expectations.
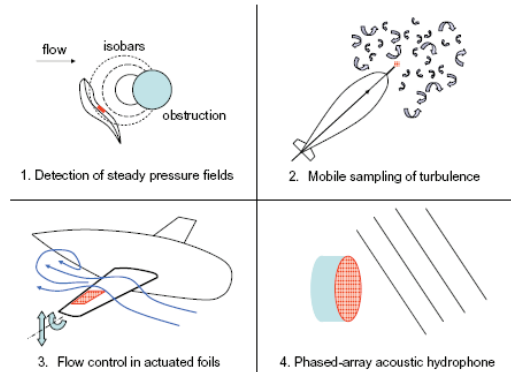

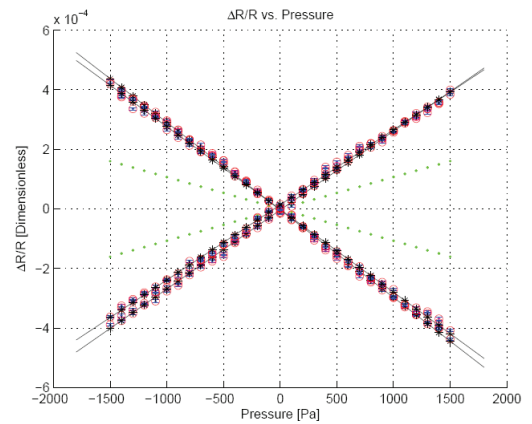**FIGURE 1:** Pressure-sensor array applications.

FIGURE 2: $\Delta R/R$ at various pressures for each of the four strain-gauge resistors on a particular diaphragm with width 2.82 mm. The circles represent data points, the asterisks and solid lines represent the best-fit lines, and the dotted lines represents the theoretical data.

Integrated Measurement of the Mass and Surface Charge of Discrete Microparticles Using a Suspended Microchannel Resonator

P. Dextras, T. P. Burg, S. R. Manalis
Sponsorship: NCI

REFERENCE

[1]   P. Dextras, T. P. Burg, and S. R. Manalis, "Integrated Measurement of the Mass and Surface Charge of Discrete Microparticles Using a Suspended Microchannel Resonator," Anal. Chem., 2009, 81 (11), pp 4517–4523.

Measurements of the mass and surface charge of microparticles are employed in the characterization of many types of colloidal dispersions. The suspended microchannel resonator (SMR) is capable of measuring individual particle masses with femtogram resolution. Here we employ the high sensitivity of the SMR resonance frequency to changes in particle position relative to the cantilever tip to determine the electrophoretic mobility of discrete particles in an applied electric field [1]. When a sinusoidal electric field is applied to the suspended microchannel, the transient resonance frequency shift corresponding to a particle transit can be analyzed by digital signal processing to extract both the buoyant mass and electrophoretic mobility of each particle (Figure 1). These parameters, together with the mean particle density, can be used to compute the size, absolute mass, and surface charge of discrete microspheres, leading to a true representation of the mean and polydispersity of these quantities for a population. We have applied this technique to an aqueous suspension of two types of polystyrene microspheres in order to differentiate them on the basis of their absolute mass and their surface charge (Figure 2). The integrated measurement of electrophoretic mobility using the SMR is found to be quantitative based on comparison with commercial instruments and exhibits favorable scaling properties that will ultimately enable measurements from mammalian cells.
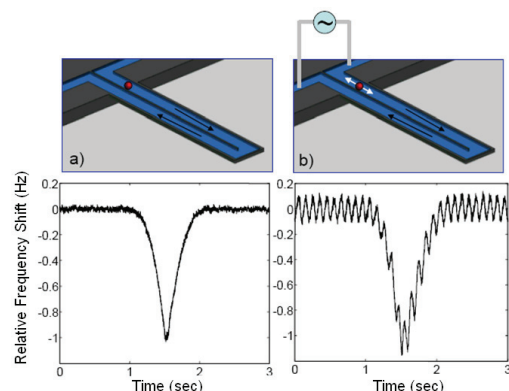

FIGURE 1: (a) A cut-away view of the fluid-filled suspended microchannel through which particles travel (top). This channel is a tunnel through the inside of the resonant cantilever structure. A transient resonance frequency time course is shown (bottom) for a 2.2μm polystyrene particle which drifts through the sensor under a small pressure gradient. The height of the peak is proportional to the particle's buoyant mass. (b) If an oscillating electric field is applied longitudinally to the channel, particles will oscillate at the same frequency due to a combination of electrophoresis and electroosmotic flow. Spectral analysis of the resulting resonance frequency time course can be performed to extract the particle's electrophoretic mobility.
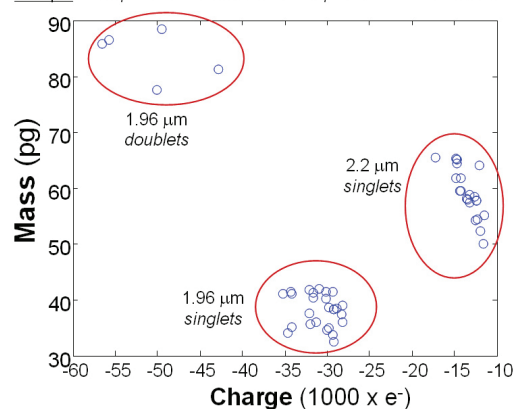
FIGURE 2: Plotting the absolute masses of individual particles against their measured zeta potential or charge reveals additional information about the population. Both scatter plots reveal two sub-populations of the more negative of the two particle types, which is not evident in the zeta potential data alone. We interpret these to be monomers and dimers of this particle type since one sub-population has a mean mass that is roughly double that of the other one at the same zeta potential. The observation that this type of particle tends to aggregate more than the other type in the mixture is supported qualitatively by the observation that these particles exhibited higher non-specific binding to the channel walls. The mass-charge scatter plot illustrates how these sub-populations are more readily differentiated on the basis of charge. It is therefore expected that integrated measurement of both the surface charge and mass distributions will provide advantages in the differentiation of complex particle mixtures.

Surface Micromachining via Digital Patterning

E. W. Lam, H. Li, V. Bulović, M.A. Schmidt
Sponsorship: DARPA, Hewlett-Packard

REFERENCES

[1]   J. Chen, V. Leblanc, S.-H. Kang, M.A. Baldo, P.J. Benning, V. Bulović, and M.A. Schmidt, "Direct patterning of organics and metals using a micromachined printhead," in *Proc. MRS Spring 2005*, San Francisco, CA, Mar./Apr. 2005, pp. H1.8:1-7

[2]   J. Feng, M. Winnik, R.R. Shivers, and B. Clubb, "Polymer blend latex films: morphology and transparency," *Macromolecules*, vol. 28, no. 23, pp. 7671-7682, Nov. 1995.

Conventional microelectromechanical systems (MEMS) fabrication relies heavily on the semiconductor manufacturing paradigm. While this model is well-suited for planar devices such as integrated circuits, it is drastically limited in the design and fabrication of three-dimensional devices such as MEMS. From a commercial viewpoint, this paradigm also poorly fits MEMS because the lower market demand makes it harder to offset the high production costs. Ridding MEMS fabrication of its reliance on such techniques may introduce several advantages, namely a wider base of substrate materials as well as decreased manufacturing costs.

Our project investigates severing MEMS fabrication from the traditional paradigm via digital patterning technologies. We have previously shown how MEMS can be used for the direct patterning of small molecular organics [1]. Using similar concepts, we have shown that surface micromachining can also be achieved.
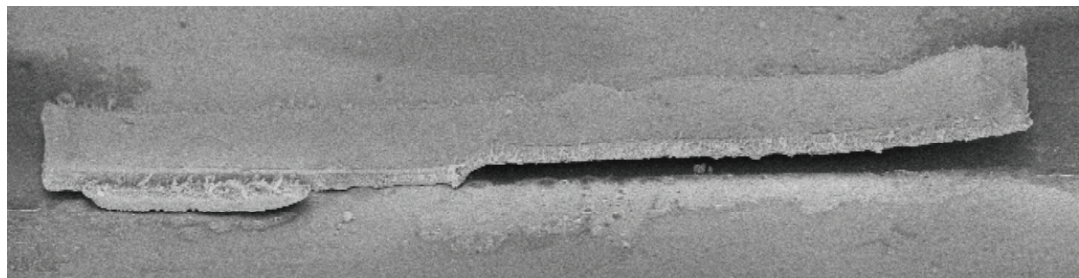
In 2007-2008, we identified a viable material set for our surface micromachining process' sacrificial and structural layers: poly-methylmethacrylate (PMMA)

and silver nanoparticles. To account for surface non-uniformity of the deposited PMMA, we employed solvent vapors to effectively lower the polymer's glass transition temperature and cause reflow at room temperatures [2]. To limit surface wetting and increase material loading of the silver nanoparticles, we deposited a PMMA reservoir to contain the silver nanoparticle solution (Figure 1). Free-standing cantilevers were fabricated (Figure 2), confirming that these techniques can be used for a surface micromachining process.

The next stage will be to fabricate additional MEMS structures and test the silver nanoparticle's mechanical properties. These properties will be used to design and fabricate a demonstration system based on our surface micromachining process. Subsequent stages will include creating a library of digital fabrication processes so that entire MEMS devices can be fabricated without the use of semiconductor manufacturing techniques.

FIGURE 1: A silver surface micromachined cantilever fabricated using direct printing.

Integration of Printed Devices and MEMS

H. Li, M. A. Schmidt
Sponsorship: DARPA, Hewlett-Packard

As part of an overall effort on Non-Lithographic Technologies for MEMS and NEMS, we are developing processes for the integration of printed MEMS and devices. The goal of this project is to demonstrate the power of a printed technology for microsystems. We have already developed a surface micromachined cantilever technology that utilizes silver as a structural material and a novel organic spacer. Further, we have developed a family of both inorganic and organic devices that can ultimately be printed. As an initial demonstration, we are building a MEMS capacitive accelerometer that integrates the silver surface micromachined proof mass and spring with a capacitive sense circuit fabricated using organic FETs.

FIGURE 1: Schematic illustration of the integration of a printed MEMS cantilever with a printed electronic device.

The MIT-OSU-HP Focus Center on Non-lithographic Technologies for MEMS and NEMS

M. A. Schmidt (in coll. with S.-G. Kim, C. G. Sodini, V. Bulović, H. L. Tuller, MIT; D. Keszler, J. Wager, OSU; J. Stasiak, Hewlett-Packard)
Sponsorship: DARPA, Hewlett-Packard

This center is part of a set of centers on MEMS/NEMS fundamentals supported by DARPA. The MIT-OSU-HP Focus Center aims to develop new methods for fabrication of MEMS and NEMS that do not use conventional lithographic techniques. The Center leverages the leading expertise of MIT and OSU in MEMS and printed devices, with the printing expertise of HP. The Focus Center is organized into four primary areas: tools, materials and devices, circuits, and demonstration systems.

In the area of tools, we are leveraging the existing thermal inkjet (TIJ) technology of HP and augmenting it with specific additional features, which expand the palette of available materials for printing. We are developing materials and devices over a broad spectrum from active materials and photonic and electronic materials to mechanical materials. In the circuits area, we are studying the behavior of the devices that can be realized in this technology with the goal of developing novel circuit architectures. Lastly, we intend to build several "demonstration" systems that effectively communicate the power of the new technologies that will emerge from this center. In the past year, the center has succeeded in demonstrating a number of the key "building blocks" for a fully printed system. Specifically, we have created printed transistors, printed optical elements (light emitters and photodetectors), printed active materials (piezoelectrics), and a printed MEMS structure (micro-cantilever). Looking forward, we will begin efforts to integrate some of these building blocks.

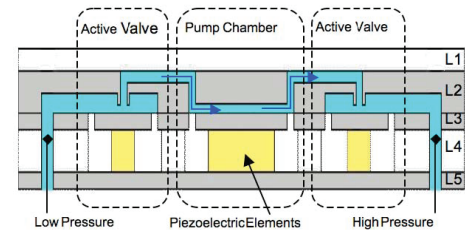# MEMS Micro-vacuum Pump for Portable Gas Analyzers

V. Sharma, M.A. Schmidt
Sponsorship: DARPA

REFERENCES

[1]   D.J. Laser and J.G. Santiago, "A review of micropumps," *Journal of Micromechanics and Microengineering*, vol. 14, no. 6, pp. 35-64, 2004.

[2]   P. Woias, "Micropumps--past, progress and future prospects," *Sensors and Actuators B: Chemical*, vol. 105, no. 1, pp. 28-38, 2005.

[3]   H.Q. Li, D.C. Roberts, J.L. Steyn, K.T. Turner, J.A. Carretero, O. Yaglioglu, Y.-H. Su, L. Saggere, N.W. Hagood, S.M. Spearing, M.A. Schmidt, R. Mlcak, and K. Breuer, "A high-frequency, high flow rate, piezoelectrically driven MEMS micro-pump," *IEEE Solid State Sensors and Actuators Workshop*, Hilton Head SC, June 2000.

[4]   A.K. Henning, "Improved gas flow model for micro-valves," *Proceedings of Transducers 2003*, Boston, MA, pp. 1550-1553, June 2003.

[5]   D.C. Roberts, O. Yaglioglu, J.Carretero, Y.-H Su, L. Saggere, and N.W. Hagood, "Modeling, design, and simulation of a piezoelectrically driven microvalve for high pressure, high frequency applications," in *Proc. SPIE–The International Society for Optical Engineering, Smart Structures and Materials 2001–Smart Structures and Integrated Systems*, Newport Beach, CA, Mar. 2001, pp. 366-380

There are many advantages to miniaturizing systems for chemical and biological analysis. Recent interest in this area has led to the creation of several research programs, including a Micro Gas Analyzer (MGA) project at MIT. The goal of this project is to develop an inexpensive, portable, real-time, and low-power approach for detecting chemical and biological agents. Elements entering the MGA are first ionized, then filtered by a quadrupole array, and sensed using an electrometer. A key component enabling the entire process is a MEMS vacuum pump, responsible for routing the gas through the MGA and increasing the mean free path of the ionized particles so that they can be accurately detected.
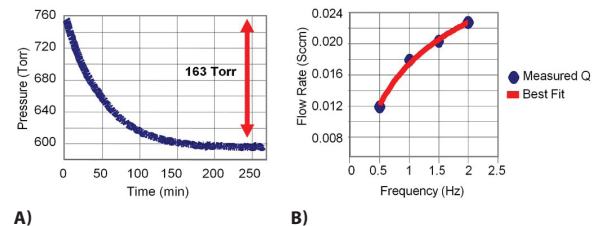
A great deal of research has been done over the past 30 years in the area of micro pumping devices [1, 2]. We are currently developing a displacement micro-vacuum pump that uses a piezoelectrically driven pumping chamber and a pair of piezoelectrically driven active-valves; the design is conceptually similar to the MEMS pump reported by Li et al. [3]. We have constructed an accurate compressible mass flow model for the air flow [4] as well as a nonlinear plate deformation model for the stresses experienced by the pump parts [5]. Using these models, we have defined a process flow and fabricated five generations of the MEMS vacuum pump over the past years and are currently working on improving the overall design.

Figure 1 shows a schematic of the pump. For ease in testing we have initially fabricated only layers 1-3 and have constructed a testing platform which, under full computer control, drives the pistons and monitors the mass flows and pressures at the ports of the device. The lessons learned from the first four generations of the pump have led to numerous improvements. Every step from the modeling, to the etching and bonding, to the testing has been modified and improved along the way. The most recent fifth generation pump test data appears in Figure 2. Figure 2a shows the measurements of the vacuum being generated in an external volume (5.6cm^3) by the micropump operating at 2Hz. The pump was able to reduce the external volume pressure by 163 Torr. Figure 2b shows the micropump-generated flow rate as a function of pumping frequency (driven in a 6-stage

cycle by a controlling microprocessor to move the gas from the input to the output). The performance of this pump compares very well with that of other similar scaled micropumps in the literature. Next, we plan to fabricate and test an improved overall design and develop a final set of models to fabricate any future micropumps to the desired specifications.

FIGURE 1: The MEMS vacuum pump schematic. Layers 1 and 4 are glass, layers 2 and 5 forming the chambers, channels, and support are silicon, and layer 3 forming the pistons and tethers is SOI silicon

FIGURE 2: a) The vacuum generation performance of the micropump. b) The pump-generated flow rate as a function of the pumping frequency.

Phase-change Materials for Actuation

Q. Guo, Y. Li, J. Kalb, C. V. Thompson
Sponsorship: Singapore-MIT Alliance

REFERENCES

[1] J.A. Kalb, Q. Guo, X. Zhang, Y. Li, C. Sow, and C.V. Thompson, Phase-Change Materials in Optically Triggered Microactuators, J. of Microelectromechanical Systems 17, 1094 (2008).

[2] Qiang Guo, Minghua Li, Yi Li, Luping Shi, Tow Chong Chong, Johannes A. Kalb, and Carl V. Thompson, Crystallization-induced stress in thin phase change films of different thicknesses, Appl. Phys. Lett., 93, 221907 (2008).

[3] Y. Li, Q. Guo, J.A. Kalb, and C.V. Thompson, Matching Glass-Forming Ability with the Density of the Amorphous Phase, Science 322, 1816 (2008).

Phase-change materials (chalcogenide alloys) are used for optical data storage in commercial phase-change memories, such as rewritable compact discs (CD±RW) and rewritable digital video disks (DVD±RW, DVD-RAM). Recently, they have also shown high potential for the development of phase-change random access memories (PC-RAMs or PRAMs), which might replace flash memories in the future.
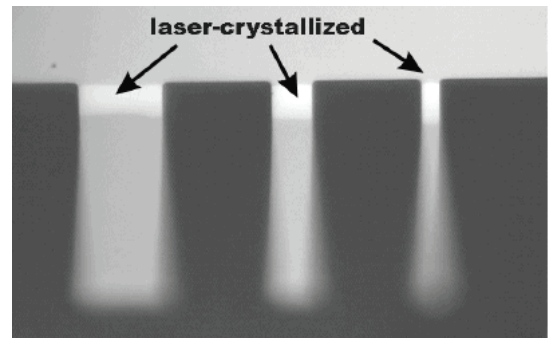
In this project, we suggest a different application of phase-change materials in optically triggered micro actuators [1]. The suggested device consists of a thin film of a phase-change material deposited on a micro-fabricated low-stress SiN cantilever. The SiN cantilevers are manufactured by chemical vapor deposition of low-stress SiN on Si wafers, patterning the SiN film using optical lithography and revealing the cantilevers using dry etching and wet etching. Amorphous thin films of phase-change materials are subsequently sputter-deposited on these cantilevers. A laser-induced crystallization in the film initiates a cantilever deflection since this transformation is accompanied by a large density change at the order of 6-9%. Then we will re-amorphize the crystalline part of the film by short laser pulses, and the cantilever tip should return to its initial position. Both the amorphous and crystalline states of phase-change materials are stable at room temperature, and the resulting device can serve as a bi-stable micro actuator.

We have also used a similar technique to investigate the stress change as a function of film thickness and capping layer [2]. This approach can be used in optimization of chalcogenides for use in PRAMS.

In addition to chalcogenides, the cantilevers used with combinatorial deposition have been used to investigate the crystallization-induced stress for a metallic amorphous alloy system (Cu-Zr). It was discovered that the magnitude of the stress change scaled with the ease of glass formation, yielding fundamental new insight into the materials requirements for amorphization [3].
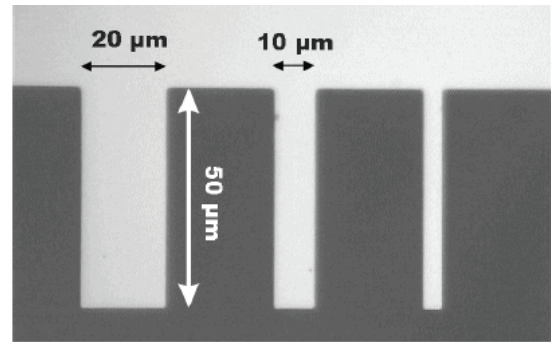
FIGURE 1: Optical micrograph of SiN cantilevers fabricated using optical lithography and dry/wet etching. An amorphous phase-change $Ge_2Sb_2Te_5$ film has been deposited on top.

FIGURE 2: The $Ge_2Sb_2Te_5$ film has been crystallized with a scanning HeNe laser near the support of the cantilevers. As a consequence, the reflectivity increases and the cantilever tip moves up by about 7.5µm, which reveals the laser-induced strain and stress in the film.

Origin and Control of Intrinsic Stresses in Metallic Thin Films for N/MEMS Applications

H. Yu, C. V. Thompson
Sponsorship: NSF

REFERENCES

[1]   F. Spaepen,"Interfaces and stresses in thin films," Acta. Materialia, vol. 48, pp. 31-42, 2000.

[2]   C. Friesen and C.V. Thompson, "Reversible Stress Relaxation during Precoalescence Interruptions of Volmer-Weber Thin Film Growth, Physical Review Letters, vol. 89, no.2, p.126103, Sept. 2002.

[3]   E. Chason, B.W. Sheldon, L.B. Freund, J.A. Floro, and S.J. Heame, "Origin of compressive residual stress in polycrystalline thin films", Physical Review Letters, vol. 88,no. 15, p. 156103, Apr.2002..

[4]   J.S. Leib, "Relationships Between Grain Structure and Stress in Thin Volmer-Weber Metallic Films," Doctoral Thesis, Massachusetts Institute of Technology, Cambridge, 2008.

Because mechanical properties strongly influence the reliability and performance of films in N/MEMS applications, understanding and controlling of the intrinsic stresses in as-deposited films is of great importance. For high-atomic-mobility metals (e.g., Au, Ag, Al, Cu) deposited on amorphous substrates, much of the observed tensile stress can be attributed to grain structure evolution during which individual islands grow, impinge, and coalesce to form a continuous film. The stress state shifts from tensile during island coalescence to compressive as the film grows past continuity (see Figure 1).

The origin of post-coalescence compressive stress has been debated extensively over the past decade. Models associated with adatom-surface [1], [2] and adatom-grain boundary [3] interactions have been proposed to explain the compressive stress generation during deposition and its relaxation during interruptions of growth. Using an in-situ stress measurement system and ex-situ TEM characterization, we have experimentally shown that, for films with the same thickness, grain size has an impact on stress behavior during a growth interruption. The relationship between the inverse of grain size and the corresponding reversible stress rise was found to be linear, with zero stress for heteroepitaxial film (interpreted as films with "infinite" grain size) (see Figure 2) [4]. This experimental result strongly indicates that the microstructure of the as-deposited film, especially the grain boundary, is critical to the origin and control of intrinsic compressive stress in these films.

Current investigations are focused on analysis of the effects of processing conditions, e.g., substrate temperature and deposition rate, on the magnitude of the residual stresses in polycrystalline films We are also investigating the use of substrate topography to control island formation and stress evolution.
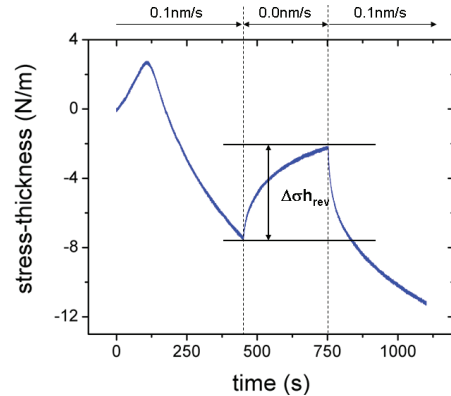
FIGURE 1: Stress-thickness curve for gold deposited at 0.1 nm/s on stress-free silicon nitride. The growth was interrupted after 450 s and resumed after 750 s.
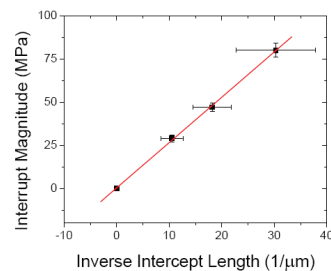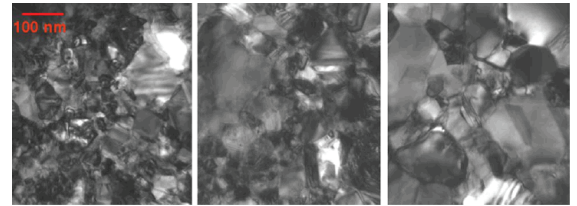
FIGURE 2: The TEM characterization and the relationship between tensile rise during interruption and the inverse grain size. As the grain size increases, the stress trends towards zero.

Microfluidic Perfusion for Modulating Stem Cell Diffusible Signaling

K. Blagović, L. Przybyla, Y.-C. Toh, J. Voldman
Sponsorship: NIH NIBIB, NSF Graduate Research Fellowship, A*STAR International Fellowship

REFERENCES

[1]   K. Blagović, L.Y. Kim, A. M. Skelley, and J. Voldman, "Microfluidic control of stem cell diffusible signaling," in *Proc. of Twelfth International Conference on Miniaturized Systems for Chemistry and Life Sciences,* San Diego, USA, Oct. 2008, pp. 677-679.

[2]   A. M. Skelley and J. Voldman, "An active bubble trap and debubbler for microfluidic systems," *Lab on a Chip,* vol. 8, pp. 1733-1737, Oct. 2008.

[3]   A. M. Skelley, and J. Voldman, "An active, integrated bubble trap and debubbler for microfluidic applications," in *Proc. of Twelfth International Conference on Miniaturized Systems for Chemistry and Life Sciences,* San Diego, USA, Oct. 2008, pp. 1360-1362.

[4]   E. Y. L. Fok and P. W. Zandstra, "Shear-Controlled Single-Step Mouse Embryonic Stem Cell Expansion and Embryoid Body-Based Differentiation," *Stem Cells,* vol. 23, pp. 1333-1342, Aug. 2005.
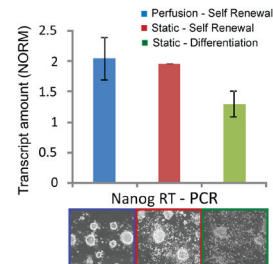
Stem cell phenotype and function are influenced by microenvironmental cues comprised of cell-cell, cell-extracellular matrix (ECM), cell-media interactions, and mechanical forces. Although conventional cell-culture techniques have been successful, they provide incomplete control of the cellular microenvironment. Our research focuses on developing microscale systems for controlling the cellular microenvironment of mouse embryonic stem cells (mESCs) to control their function.

To modulate cell-media interactions, we have developed a two-layer PDMS microfluidic device that incorporates a valve architecture, debubblers, and cell culture chambers, allowing for a rich set of culture conditions on the same chip [1-3]. We are using our microfluidic system to determine the minimal media sufficient for mESCs to maintain their self-renewal characteristics under constant flow. Upon growing mESCs in defined, serum-free media conditions under perfusion, we have observed a change in the preponderance and the heterogeneity of stem cell markers. Using a combination of assays, we have observed similar or upregulated levels of the stem cell marker Nanog, as well as a more stem cell-like morphology of cells under perfusion (Figure 1).

The use of ESCs for clinical therapeutic applications requires expansion of the pluripotent cells. This usually necessitates the use of a bioreactor where the cells are subjected to mechanical forces: fluid shear stresses [4]. We are quantitatively investigating the effect of fluid shear stress on ESC self-renewal by using a 1x6 logarithmic flow rate microfluidic device. By specifying the dimensions of the flow rate-setting resistor channels, we were able to apply shear stress varying by a factor of 4 across

chambers, enabling us to simultaneously study shear stress effects on mESC self-renewal over a range of 1024× (Figure 2a). Initial results show that mESC proliferation is negatively correlated to shear stress over a range of 0.016 to 16 dynes/cm² (Figure 2a).
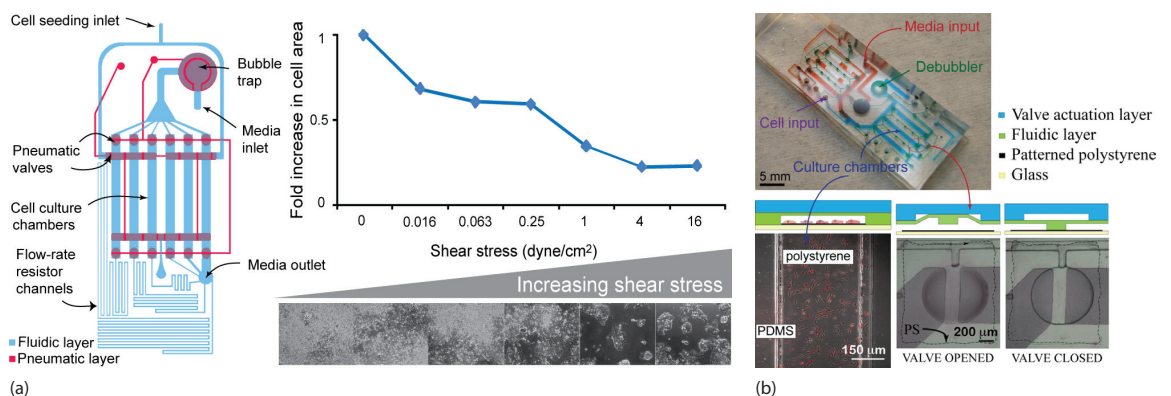
ESCs dynamically interact with their extracellular matrix (ECM) and culture substrate. In particular, different substrates adsorb ECM differently, which in turn affects cell attachment and function. Standard culture techniques typically utilize *tissue culture polystyrene* (TCPS), a treated polystyrene substrate that promotes ESCs attachment. We developed a process that integrates micro-patterned polystyrene onto glass substrates, combining the cell culture compatibility of polystyrene with the fabrication compatibility of glass (Figure 2b). This process integrates cell culture surfaces directly within a device and preserves the standard microfluidic assembly process of plasma bonding. We have demonstrated a simple technique for realizing multi-functional polystyrene patterns for the fabrication of complex, highly integrated microfluidic cell culture platforms.

FIGURE 1: Cells grown for 5 days in a device and static culture. Quantitative analysis for self-renewal marker Nanog (RT-PCR) and corresponding phase images of mESC colonies.

(a)

(b)

FIGURE 2: (a) 1×6 logarithmic flow-rate microfluidic device for studying the effects of shear stress on mESCs self-renewal. Schematic of a device (a, left). Proliferation of mESCs, experiencing a broad range of shear-stress values, cultured for 72 hours in a device (a, right). (b) Image of a 2-layer microfluidic perfusion device (b, top). Applications of micro-patterned polystyrene (PS): PS patterned cell-culture chambers with NIH-3T3 mouse fibroblasts (b, bottom left) and normally closed valves with PS patterned valve seat (b, bottom right).

Microfluidic Control of Cell Pairing and Fusion

M. Hoehl, A. Skelley, J. Voldman
Sponsorship: NIH

REFERENCES

[1]   A. M. Skelley, O. Kirak, H. Suh, R. Jaenisch, and J. Voldman, "Microfluidic Control of Cell Pairing and Fusion," *Nature Methods,* vol. 6, pp. 147-52, 2009.

Currently, several different methods have been used to reprogram somatic cells to an embryonic stem-cell-like state, including somatic cell nuclear transfer, forced expression of transcription factors, and cell fusion. Cell fusion is an appealing method by which to study reprogramming as the delivery of cells is easily visualized. However, conventional methods to fuse cells *en masse* do not control the pairing between the cell populations, resulting in heterogeneous output populations that must be further purified.

We have developed a microfluidic system in which thousands of ESCs and somatic cells (SCs) are properly paired and immobilized, resulting in a high number of one-to-one fusions that can be clearly identified for further studies [1]. The device consists of thousands of microscale cell traps in a millimeter-sized area. The traps consist of larger frontside and smaller backside capture cups made from a transparent biocompatible polymer. The key to pairing cells efficiently is to load them sequentially in a 3-step loading protocol enabling capture and pairing of two different cell types (Figure 1). The geometry of the capture comb precisely positions the two cells, and flow through the capture area keeps the cells in tight contact in preparation for fusion. With this approach we have obtained pairing efficiencies of ∼70%.

The device is compatible with both chemical and electrical fusion, and, in agreement with the literature, we have obtained higher performance with electrofusion. When we compared fusion performance in our device to commercial approaches, we obtained significant improvements in overall performance for both PEG-mediated fusion and electrofusion. Specifically, we have measured fusion efficiencies of ∼80% in our device using electrofusion, about 5× greater than that obtained in commercial systems. We are also able to remove fused cells from the device and culture them, demonstrating that the device creates viable fused cells (Figure 2a-b). Finally, by fusing mouse embryonic stem cells (mESCs) with mouse embryonic fibroblasts (mEFs, a somatic cell type), we have demonstrated the ability to reprogram the somatic cells to a pluripotent state as evidenced by morphology, alkaline phosphatase staining (Figure 2c), and activation of an oct4-GFP reporter present in the somatic cell genome (Figure 2d).
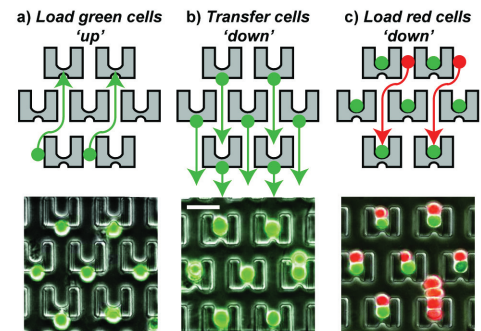
FIGURE 1: Three-step cell loading protocol. (a) Cells are first loaded "up" towards the smaller backside capture cup. (b) The direction of the flow is reversed, and the cells are transferred "down" into the larger frontside capture cup 2 rows below; scale bar, 50 mm. (c) The second cell type is loaded in from the top, and cells are captured in front of the first cell type.
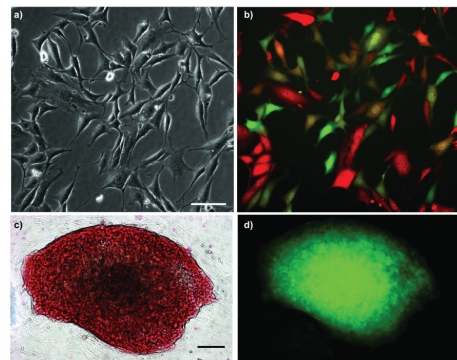
FIGURE 2: Functionality of fused cells. (a-b) Phase and fluorescent image of DSRed/EGFP fibroblasts at day 4 after fusion in the microfluidic device. scale bar, 100 mm. (c-d) Double-resistant hybrids between Hygromycin B-resistant mESCs and Puromycin-resistant mEFs after fusion in the microfluidic device, showing ESC-like morphology, positive alkaline phosphatase, staining, and reactivation of endogenous Oct4-GFP reporter; scale bar, 100 mm.

Flexible Multi-site Electrodes for Moth Flight

W. M. Tsang, S. Murray, A. I. Akinwande, J. Voldman
Sponsorship: DARPA

REFERENCES

[1]   W.M. Tsang, Z. Aldworth, A. Stone, A. Permar, R. Levine, J.G. Hildebrand, T. Daniel, A.I. Akinwande, and J. Voldman, "Insect flight control by neural stimulation of pupae-implanted flexible multisite electrodes," Micro Total Analysis Systems, 2008, pp. 1922-24.

Significant interest exists in creating insect-based Micro-Air-Vehicles (MAVs) that would combine advantageous features of insects—small size, effective energy storage, navigation ability—with the benefits of MEMS and electronics—sensing, actuation and information processing. The key part of the insect-based MAVs is the stimulation system, which interfaces with the nervous system of the insect to bias the insect's flight path.

In this work, we have developed a flexible split-ring electrode (FSE) for insect flight control; the FSE uses a set of electrodes arranged around a split ring to provide circumferential stimulation around an insect's nerve cord (Figure 1). The FSE is made of two layers of polyimide with gold sandwiched in between in a split-ring geometry using standard MEMS processing. The stimulation sites are located at the each end of protruding tips that are circularly distributed inside the split-ring structure. These protruding tips penetrate through the cuticle tissues of the nerve cord and enable stimulation on the axon-rich region of the nerve cord.

We have been able to insert the electrode into pupae of *Manduca sexta* as early as 7 days before the adult moth emerges, and we are able to stimulate multi-directional graded abdominal motions in both pupae and adult moths. The direction of the abdominal movements depends on the particular pair of stimulation sites excited. The pupal implantation allows for tissue growth around the FSE before the adult moth emerges, which enhances the attachment of the FSE. Also, as compared to the adult moth, the body of the pupae is relatively immobile, easing the difficulty of insertion surgery. Finally, we have demonstrated that the FSE is able to stimulate abdominal motion that can in turn cause ruddering to alter adult moth flight path (Figure 2) [1].
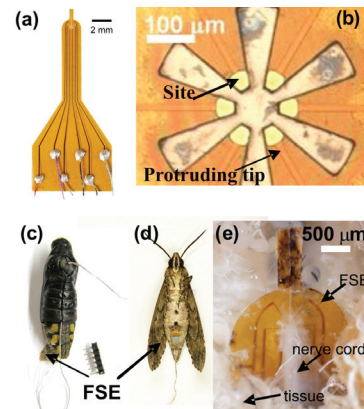
FIGURE 1: (a) Image of the FSE with wire connection; (b) Close-up image of the FSE at the split-ring region; (c) Image of a pupa with inserted FSE; (d) Enclosed adult moth with FSE inserted at the pupal stage; (e) Image of dissected adult moth showing the growth of connective tissue around the FSE.
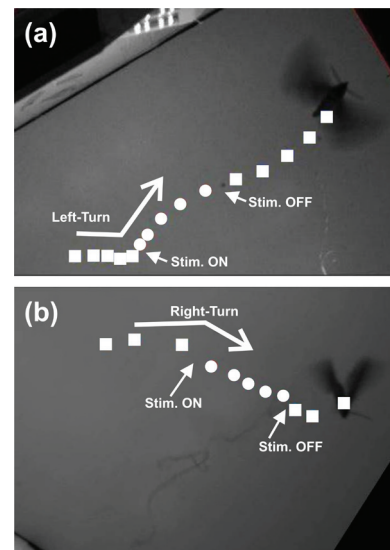
FIGURE 2: Images showing the loosely tethered moth that has been stimulated to perform (a) left and (b) right turns following the stimulation of the FSE. The flight path of the moth with and without FSE stimulation are tracked by solid circle (●) and solid square (■) dots, respectively.

Measuring the Effects of Electric Fields on Cell Phenotype

S. P. Desai, J. Voldman
Sponsorship: NIH, Singapore-MIT Alliance

REFERENCES

[1]   B.M. Taff, S. P. Desai, and J. Voldman, *Applied Physics Letters*, vol. 97, no. 8, pp. 084102-3, 2009.

[2]   M. D. Vahey and J. Voldman, *Analytical Chemistry*, vol. 81, no. 7, pp. 2446-2455, 2009.

[3]   S. P. Desai and J. Voldman, *Proceedings of Twelfth International Conference on Miniaturized Systems for Chemistry and Life Sciences*, 2008, pp. 1308-1310.

One overarching goal of our research group involves using electric fields to manipulate, position, and ultimately sort living biological entities [1], [2]. To enable such exquisite control over living organisms, we leverage a technique called dielectrophoresis (DEP), which uses spatially non-uniform electric fields to "push" or "pull" cells towards or away from electrodes. The processing of biological samples is more readily achieved using systems on the length-scale of the samples themselves. Such biological microelectromechanical systems, or BioMEMS, enable integrated sample preparation and analysis; they leverage techniques such as DEP to enable cell manipulation. Hence, it is imperative that we understand the effects of DEP manipulation on cell physiology to determine whether DEP manipulation itself can alter particular phenotypes of interest and confound downstream biological assays. To this end, we have developed a microfabricated, high-content screening (HCS) platform that can apply a large number of different electrical stimuli to cells and then monitor the molecular effects of those stimuli using automated fluorescence microscopy. The platform consists of a chip with individually addressable arrayed electrodes and support electronics to generate the desired waveforms (Figure 1). Mammalian cells are seeded on the chip and then the entire assembly is clamped and placed in a standard cell culture incubator, where a computer-controlled custom-designed switch box automatically and autonomously applies arbitrary stimulation waveforms (varying voltage, frequency, and duration) to individual electrode sites. Since this platform uses transparent electrode structures, it can equally be used with both inverted and fluorescent microscopy techniques.

Using this HCS platform, we have been able to elucidate the response of cells to electric fields using a custom-designed live-cell stress sensor. This stress sensor was designed using transfection and cloning techniques, and it forms the basis for the read-out of our biological assay. Stressful events in the environment around the cells, such as temperature elevation (due to Joule heating) and the generation of oxygen radicals are sensed by our stress sensor and reported as a distinct fluorescence level. These fluorescent signals are collected for individual cells using automated microscopy and quantified using image-processing algorithms. The results obtained from one such set of experiments are displayed in Figure 2 (adapted from [3]). This HCS platform enables the molecular-level biological assays across a very wide range of electric field conditions, a feat challenging to accomplish with previously developed systems or assay platforms.
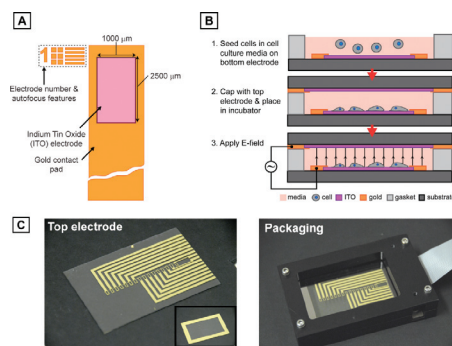
FIGURE 1: HCS platform. (A) Top-down schematic of 16 individually addressable transparent indium-tin oxide (ITO) electrodes. (B) Seeding of cells on electrodes and running the screening assay. (C) Images of bottom electrode (left panel) and top electrode chips (inset). Image of packaged device (right panel), showing bottom electrode chip visible through transparent top electrode.
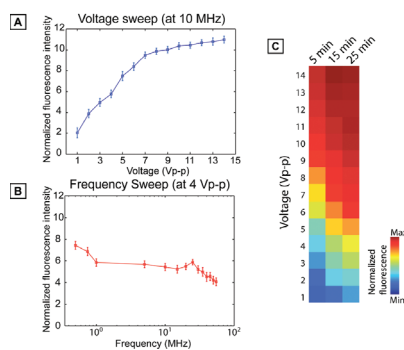
FIGURE 2: Electric-field effects. (A) The voltage sweep shows a dramatic increase in cellular stress with increase in voltage. (B) A frequency sweep indicating that cells are stressed at low frequencies (due to radical generation). (C) A heat map showing a voltage sweep for different durations of field exposure. Longer durations of exposure show increased cellular stress levels.
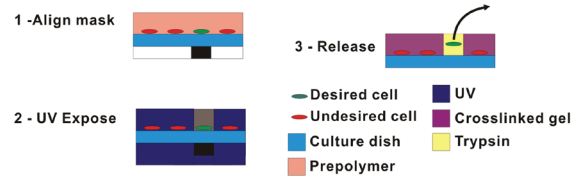
Image-based Sorting of Cells

J. R. Kovac, Y. Gerardin, B. M. Taff, J. Voldman

This research involves the development of architectures for screening complex phenotypes in biological cells. We augment microscopy with the ability to retrieve cells of interest. This capability will permit cell isolation on the basis of dynamic and/or intracellular responses, enabling new avenues for screening. Currently, such sorts require expensive, specialized equipment, widely prohibiting such sorts.

We have explored microfabricated/microfluidic approaches to cell sorting. These approaches employed purely dielectrophoretic (DEP) trap arrays [1], passive hydrodynamic trap arrays with active DEP-based cell release [2], and passive microwell arrays with optical cell release to permit sorting of non-adhered cells [3]. We recently developed a photolithography-inspired method that allows sorting of adherent cells without the use of microfluidics [4], illustrated in Figure 1. Here we plate adherent cells in a dish and assay them, identifying the locations of cells of interest. We then use a computer and standard office printer to automatically generate a transparency mask. After alignment of the transparency mask to the back of the cell culture dish, opaque mask features reside beneath desired cells. We then add a prepolymer to the dish, containing cell culture media, a UV-photoinitiator, and poly(ethylene glycol) diacrylate (PEGDA) monomer. Next we use a standard fluorescence lamp to shine UV light through the mask, crosslinking a hydrogel over all unmasked locations and encapsulating all undesired cells. Desired cells can be enzymatically released (Figure 2) and re-captured. Our sorting process requires standard equipment found in biology labs and inexpensive reagents (<$10 per experiment), simplifying widespread adoption.

We have demonstrated cell release from 500-μm-diameter wells, as well as the isolation of perfectly pure, viable target cells from a background population of undesired cells. Further efforts will reduce well size, enabling the sorting of denser cell populations. The simplicity and inexpensiveness of our method will allow for widespread dissemination and new cell sorting paradigms.

REFERENCES

[1]   J. R. Kovac, B. M. Taff, J. Voldman, "Enabling technologies for image-based cell sorting," in ch. "Microdevices in Biology and Medicine," Y. Nahmias, S. Bhatia, Eds. in *Methods in Bioengineering*, M. Yarmush, R. Langer, Eds. to be published.

[2]   B. M. Taff, S. P. Desai, J. Voldman, "Electroactive hydrodynamic weirs for micro-particle manipulation and patterning," *Applied Physics Letters,* to be published.

[3]   J. R. Kovac and J. Voldman, "Image-based cell sorting using optofluidics," in *Digest of the IEEE/LEOS Summer Topical Meetings*, 2008, pp. 193-194.

[4]   J.R. Kovac and J. Voldman, "Microscopy-based sorting of adherent cells using photopolymerization-activated cell sorting (PACS)," presented at the *Biomedical Engineering Society annual meeting*, St. Louis, MO, 2008.

FIGURE 1: Schematic of sorting method. 1) Mask is aligned such that opaque features reside behind desired cells; prepolymer is added. 2) UV light crosslinks polymer in exposed regions, encapsulating undesired cells. 3) Un-encapsulated desired cells are released and reclaimed.
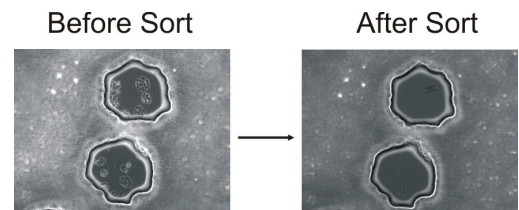
FIGURE 1: Image showing a 500-µm-diameter well surrounding desired MCF7 cells before and after sorting; cells in wells are released while cells within hydrogel remain.

Cell Micropatterns for Studying Autocrine Signaling

S. Sampattavanich, N. Mittal, J. Voldman
Sponsorship: NIH NIBIB, Singapore-MIT Alliance

REFERENCES

[1] S. Sampattavanich, J. Voldman, "Examining the effective autocrine length scale using stencil cell patterning," presented at *BMES Annual Fall Meeting*, St. Louis, USA, 2008.

[2] N. Mittal, J. Voldman, "Exploring cell-cell communication in mouse embryonic stem cell culture using Bio Flip Chips," presented at *6th Annual Meeting of the International Society for Stem Cell Research*, Philadelphia, USA, 2008.

[3] S. Sampattavanich, B. M. Taff, S. P. Desai, and J. Voldman, "Organizing complex multicellular constructs using stencil-delineated electroactive patterning (S-DEP)," presented in *Proc. Twelfth International Conference on Miniaturized Systems for Chemistry and Life Sciences,* 2008, pp. 567-69.

Autocrine signaling plays a key role in tumorigenesis and in the maintenance of various physiologic states. Due to its intrinsic, closed-loop nature, autocrine signaling is, however, difficult to investigate experimentally. Our research involves the use of cell- patterning techniques to investigate the role of autocrine signaling during *in vitro* maintenance of embryonic stem cells, stem cell differentiation, and uncontrolled expansion of cancer cells.
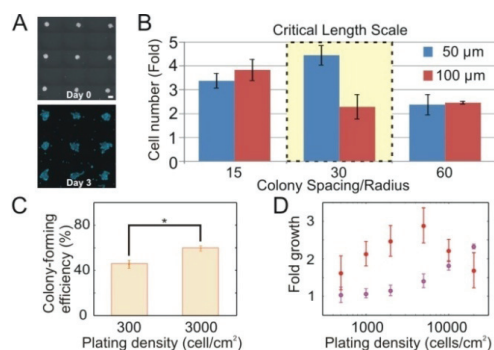
First we use stencil cell patterning to examine the spatial distribution of autocrine systems. Typical techniques to quantify autocrine signaling rely on bulk measurement of autocrine pathway activation using randomly plated cells. Such random cell positioning usually masks the effects of local ligand concentration gradients, reducing the chance to observe spatially varying cell responses. We fabricated regular arrays of cell patches with varying colony size and spacing and generated graded levels of autocrine ligands in space while maintaining the same global ligand concentration (Figure 1A). Using the TGFα/EGFR paradigm in A431 cells as our model, we have determined the effective length scale where autocrine signaling contributed to promote growth of adjacent cell patterns (Figure 1B) [1]. We are applying the developed platform to determine the contribution of autocrine signaling in preserving a homogeneous population of mouse embryonic stem cells (mESCs) *in vitro*.

Expanding on our previous work on Bio Flip Chips, we have used them to create patterns of single cells at varying densities [2]. We then studied the effects of plating density on the colony-forming efficiency of mESCs and found that the colony-forming efficiency increases with density (Figure 1C). We have confirmed this result by performing growth assays in a traditional well-plate format and in a defined medium. In this second set of assays, we found that the growth of mESCs increases with density (for a certain range), both in the first 24 hours and in the next 24 hours after plating of cells (Figure 1D). Finally, we checked that medium that has been conditioned by cells enhances the growth of mESCs. Together, these results prove that mESCs produce at least one diffusible factor that aids survival.

In addition to localization of a single cell type on the substrate, we have also developed a novel technique to fabricate complex heterotypic patterns-within-patterns [3]. Stencil-delineated electroactive patterning (S-DEP) combines dielectrophoresis (DEP) and stencil patterning to create cell clusters with customizable shapes, positions, and internal cell organization (Figure 2). Stencils define overarching tissue-like construct geometries, and negative-dielectrophoretic forcing guides subgroupings of cells to desired positions within constructs. The S-DEP enables correlation of cells' cluster location to phenotype and provides avenues for creating mosaic tissue-like constructs of phenotypically or genetically distinct cells. Such diversified chimeric cell clusters help us evaluate the impact of diffusive signaling on stem-cell differentiation.

FIGURE 1: A) Stencil cell patterning is used to construct regular arrays of A431 cells with defined colony size and spacing at day 0 and day 3. Scale bar = 200 μm. B) Change in cell number of A431 cells for different geometric configurations. Error bars represent 95% confidence intervals. The result shows elevated cell growth at the colony spacing of 30 colony radii. C) Colony-forming efficiency increases with plating density. D) Fold growth increases with density on Day 0-1 (purple) and Day 1-2 (red).
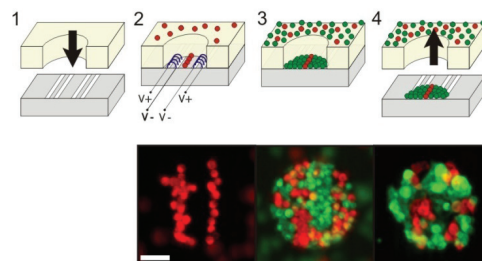
FIGURE 2: The S-DEP procedure. (1) A PDMS stencil is placed over an electroactive substrate. (2) The first cell population (stained with DiI) is seeded onto the device with the electrodes on. (3) With electrodes off, the second cell population (stained with DiO) is loaded onto the device after attachment of the first cell population. (4) After attachment of the cells, the stencil is removed, leaving behind tissue-like constructs with internally patterned subdomains. Scale bar = 50 μm.

Iso-dielectric Separation of Cells and Particles

M.D. Vahey, J. Voldman

REFERENCES
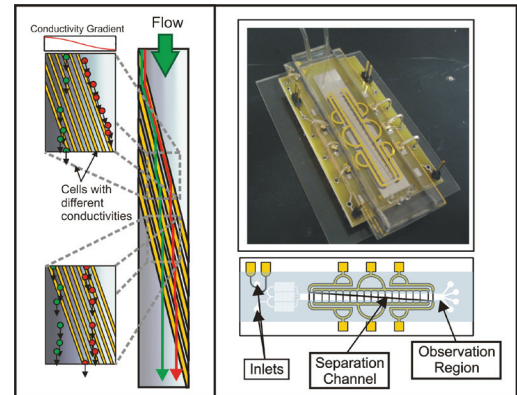
[1] H.A. Pohl and J.S. Crane, "Dielectrophoresis of cells," *Biophysical Journal*, vol. 11, pp. 711-727, 1971.

[2] M.D. Vahey and J. Voldman, "An Equilibrium Method for Continuous-Flow Cell Sorting Using Dielectrophoresis," *Analytical Chemistry*, vol. 80, no. 9, pp. 3135-3143, 2008..

[3] M.D. Vahey and J. Voldman, "Iso-dielectric Separation: A new method for the continuous-flow screening of cells," *Micro Total Analysis Systems '06*, vol. 2, pp. 1058-1060, 2006.

[4] P.R.C. Gascoyne and J. Vykoukal, "Particle Separation by Dielectrophoresis," *Electrophoresis*, vol. 23, pp. 1973-1983, 2002.

[5] M.D. Vahey and J. Voldman, "High-Throughput Cell and Particle Characterization Using Isodielectric Separation," Analytical Chemistry, vol. 81, no. 7, pp. 2446-2455.

The development of new techniques to separate and characterize cells with high throughput has been essential to many of the advances in biology and biotechnology over the past few decades. Continuing or improving upon this trend – for example, by developing new avenues for performing genetic and phenotypic screens – requires continued advancements in cell sorting technologies. Towards this end, we are developing a novel method for the simultaneous separation and characterization of cells based upon their electrical properties. This method, iso-dielectric separation (IDS), uses dielectrophoresis (the force on a polarizable object [1]) and a medium with spatially varying conductivity to sort electrically distinct cells while measuring their effective conductivity (Figure 1). It is similar to iso-electric focusing, except that it uses DEP instead of electrophoresis to concentrate cells and particles to the region in a conductivity gradient where their polarization charge vanishes [2],[3].
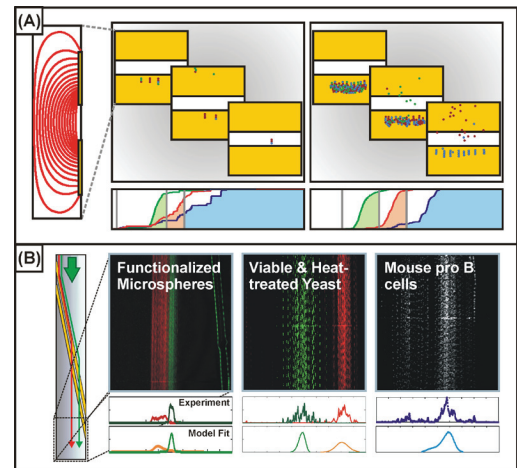
While dielectrophoresis has been widely used in cell separation [4], iso-dielectric separation offers a unique combination of features that could be potentially enabling for new genetic screens. It is continuous-flow, capable of parallel separations of multiple (>2) subpopulations from a heterogeneous background, and label-free. Additionally, in contrast to many other separation techniques, IDS leverages physical interactions between particles as they are separated to achieve better performance, and it is thus ideally suited to operation at high particle concentrations with correspondingly high throughput (Figure 2A). Finally, using IDS as a tool for cell characterization could identify electrical phenotypes and map them to specific genes. This improved understanding of the relationship between a cell's genotype and its physical properties is critical for developing new screens. We have demonstrated the separation and characterization of particles ranging from polystyrene beads, to the budding yeast *Saccharomyces cerevisiae*, to mouse pro B cells (Figure 2B), representing three orders of magnitude in particle volume ($\sim$1-1000 μm^3) and conductivity ($\sim$0.001–1 S/m) [5].

FIGURE 1: (Left) Illustration of IDS, depicting cells with different electric properties following different trajectories in a conductivity gradient. (Top right) Photograph of an assembled device. (Bottom right) Schematic of the device highlighting its primary components.

FIGURE 2: (A) Simulation illustrating performance improvement at higher particle concentrations. Larger numbers of particles (right panel) exhibit elution curves with less overlap, indicating higher separation purity. (B) Separation and characterization of cells and particles by measuring the spatial distribution of cells as they exit the device under different conditions.

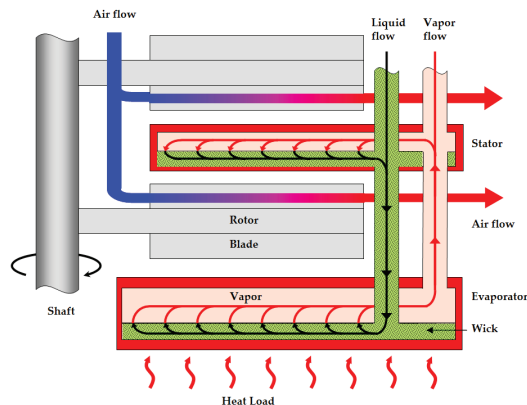# Fully Integrated Air Pumped Heat Exchanger (PHUMP)

J. Allison, A. Kariya, C. Koveal, D. Jenicek, M. McCarthy, E. N. Wang, J. G. Brisson, J. H. Lang, S. Jacobson
Sponsorship: DARPA, Lockheed Martin

The ever-increasing computational power of modern electronics entails an associated increase in heat generation in the chip; microprocessors without a thermal management system are easily capable of melting themselves. Exotic thermal management systems such as liquid cooling allow high thermal power densities but require large volumes and complex implementations. The Fully Integrated Air-Pumped Heat-Exchanger (PHUMP) heat sink allows this cost-effective technology to keep pace with the cooling demands of the advancing electronics industry.

The PHUMP will provide reduced thermal resistance and reduced power demand in a compact volume. It will be designed to operate in a range of thermal and mechanical shock environments, for an extended period of time. These goals will be achieved by incorporating heat pipes into the extended surface of the heat sink as well as incorporating fan rotors along each wall of the extended surface to maximize heat transfer. Heat pipes are enclosed systems that have a very high effective thermal conductivity by generating a two-phase flow in a working fluid contained within them [1], [2]. The improved heat transfer to the extended surface allows the PHUMP to operate at lower speeds and generate less mass flow than traditional air-cooled heat sinks. This improved heat transfer reduces the power required to turn the fan and allows the PHUMP to achieve high coefficients of performance.

REFERENCES

[1] A. Faghri, *Heat Pipe Science and Technology*. Boca Raton: Taylor & Francis Group, 1995.

[2] A. F. Mills, *Heat Transfer*.Upper Saddle River: Prentice Hall, 1999

FIGURE 1: Schematic view of one layer of the PHUMP. Air enters axially from above and is blown radially outwards by the fan. Air removes heat from the thermal stators as it passes over them. The stator is the condensing section of a heat pipe whose evaporator is adjacent to the heat load. The condensers and evaporator are connected by vertical pipes.
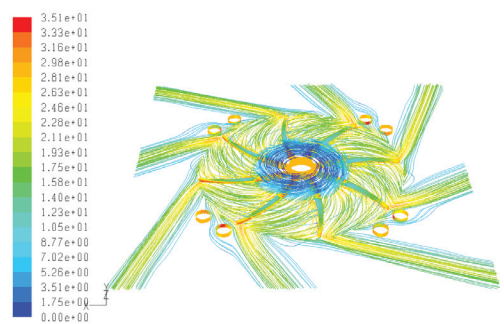
FIGURE 2: A CFD simulation of airflow through a single layer of the PHUMP. Pathlines of airflow are colored by temperature. One rotor with 8 blades is visible, along with sections of the vertical pipes that transfer the working fluid between the condensers and evaporator. Surfaces are colored by static pressure.
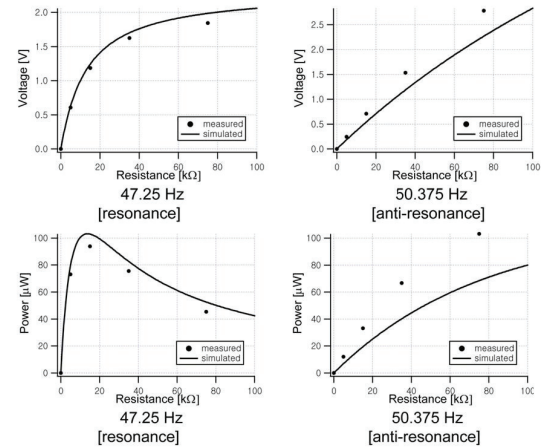
Model-based Design of MEMS Vibration-energy-harvesters for Wireless Sensors

M. Kim, W. S. Kim, M. Hoegen, S.-H. Kim, B. L. Wardle

REFERENCES

[1]   N.E. duToit and B.L. Wardle, "Experimental verification of models for microfabricated piezoelectric vibration energy harvesters," *AIAA Journal*, vol. 45, no. 5, May 2007.

[2]   M. Kim, M. Hoegen, W. S. Kim, S.-H. Kim, J. Dugundji· and B. L. Wardle· "Proof mass modeling considerations in cantilevered piezoelectric vibration energy harvesters", *Mater. Res. Soc. Symp. Proc.* vol. 1120, 2009.

[3]   N.E. duToit, B.L. Wardle, and S.-G. Kim, "Design considerations for MEMS-scale piezoelectric mechanical vibration energy harvesters," *Integrated Ferroelectrics*, vol. 71, pp. 121-160, 2005.

[4]   N.E. duToit and B.L. Wardle, "Performance of microfabricated piezoelectric vibration energy-harvesters," *Integrated Ferroelectrics*, vol. 83, pp.13-23, 2006.
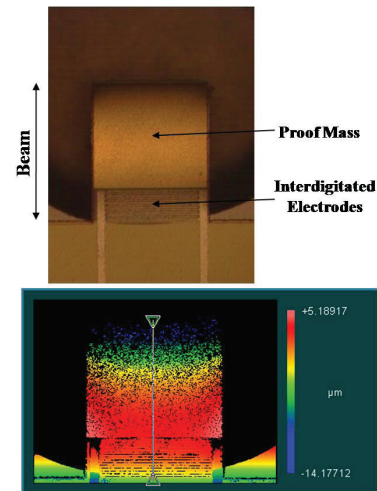
The recent development of "low power" (10s-100s of μW) sensing and data transmission devices, as well as protocols with which to connect them efficiently into large, dispersed networks of individual wireless nodes, has created a need for a new kind of power source. Embeddable, non-life-limiting power sources are being developed to harvest ambient environmental energy available as mechanical vibrations, fluid motion, radiation, or temperature gradients. While potential applications range from building climate control to homeland security, the application pursued most recently has been that of structural health monitoring (SHM), particularly for aircraft. This SHM application and the power levels required favor the piezoelectric harvesting of ambient vibration energy. Current work focuses on harvesting this energy with MEMS resonant structures of various geometries. Coupled electromechanical models for uniform beam structures have been developed to predict the electrical and mechanical performance obtainable from ambient vibration sources. The optimized models have been verified by comparison to tests on a macro-scale device both without [1] and with a proof mass at the end of the structure (Figure 1) [2]. A non-optimized, uni-morph beam prototype (Figure 2) has been designed and fabricated [3], [4]. Design tools to allow device optimization for a given vibration environment have been under detailed investigation considering various geometries of the device structures and fabrication constraints, especially in microfabrication. Future work will focus on fabrication and testing of optimized uni-morph and proof-of-concept bi-morph prototype beams. System integration and development, including modeling the power electronics, will be included.

FIGURE 1: Model predictions vs. experimental results: voltage (upper) and power (lower) vs. varying electrical load resistance at resonance and anti-resonance. [2]

FIGURE 2: Top-down views of fabricated cantilevered MEMS piezoelectric harvester. An SEM of a prototype uni-morph energy harvester device (upper) and ZYGO image of the same device (lower) for curvature measurement.